AN EXPERIMENTAL INVESTIGATION OF CYCLICALLY, AXIALLY LOADED PILES IN SAND

by

S.J. COWBURN
B.Sc. (Eng.) in Civil Engineering
University of Cape Town

A thesis submitted to the University of Cape Town in partial fulfilment of the requirements for the degree of Master of Science in Engineering

Department of Civil Engineering
University of Cape Town

August 1993

DECLARATION

I, Sean John Cowburn, hereby declare that this thesis is my own work and that it has not been submitted for a degree at any other university.

Signed by candidate

S J COWBURN

August 1993

ACKNOWLEDGMENTS

I would firstly like to express my sincere appreciation to my supervisor, Dr Friedrich Scheele, for his guidance, support, enthusiasm and valuable help throughout the research program. His support made the difficult times and many problems seem surmountable.

Many thanks are due to my laboratory assistant, James George, for his help during preparation of the experiments. He always maintained a jovial attitude even though at times the work was laborious and strenuous. The assistance of the other laboratory staff is acknowledged.

Without the help and continued support of Eike von Guerard and his workshop staff this research would not have been possible. I would like to express my gratitude to them all for their high standard of work.

The support of Peter Stoppel of Rosond (Cape) in supplying the pile casings, grouting equipment and operator is much appreciated. The research program depended entirely on his continued support.

I would also like to thank my family and fellow students for their support and encouragement during the difficult times experienced over the years. A special word of thanks is due to Cameron Howie for his invaluable assistance and expertise in the development and coding of the computer program.

Finally, I would like to express my thanks to Gordon Robertson of Hill Kaplan Scott for his assistance in soil testing, Dave Train of ABE for his donation of Bidim and Optima Hydraulics for their help in maintaining the testing equipment.

SYNOPSIS

The research work involved the installation and cyclic load testing of large-scale pressure-grouted, instrumented piles in sand in the laboratory. The major objective of this experimental investigation was to establish the effects of the mean cyclic load level and amplitude on the pile behaviour during cyclic loading. Of particular interest was the study of the skin friction distributions along the pile shafts in order to understand the processes involved. Cyclic loading was limited to one-way loading in load-controlled mode.

A literature review showed a lack of experimental data on the cyclic behaviour of large-scale pressure-grouted piles. The results of a number of small model tests in sand are discussed and the major trends of pile performances are highlighted to facilitate comparison of the observations made in this research. It was found that no definite testing procedure for cyclically-loaded piles is common to the various investigations.

A research program and procedure of load applications was therefore developed to allow the isolation of the individual influences of the most significant cyclic parameters, the mean cyclic load level and the amplitude. In total 12 piles were installed using the same sand preparation and pile installation techniques. The tests only varied with regard to the applied loading procedure.

The pile installation commenced with the driving of 76mm diameter open-ended steel casings into a 3m deep homogeneous bed of compacted sand using a drop weight pile driver. The 2.2m and 2.4m long piles were then cast using the method of pressure grouting. Certain piles were instrumented with strain gauges placed at various levels along the reinforcing bar.

During testing the displacements and loads were continuously recorded with the help of a computer-controlled, data acquisition unit.

Static load tests determined the ultimate load capacity of the piles. During cyclic tests the cyclic loads were applied sinusoidally at a frequency of 0.25Hz by a servo-controlled loading device. Variation in loading consisted of combinations of mean cyclic load levels (30kN to 120kN) and amplitudes (10kN to 30kN). The maximum number of load cycles to which a pile was exposed, was 389 000.

The effects of the load amplitude on the pile performance were found to be more significant than the mean cyclic load level. The results showed that for low amplitude piles (5% of ultimate load), at every experienced mean cyclic load level, little pile displacement (penetration) into the sand bedding occurred during the test periods. The rates of penetration decreased to reach almost constant and 'stable' low values. The stiffness modulus of the system, derived from the load-displacement behaviour (hysteresis loops) of the pile head, displayed no significant degradation. The skin friction along the pile shaft increased to reach peak values which remained relatively constant throughout cyclic loading. Point resistance increased only gradually to attain a constant value.

The application of high amplitudes (15% of ultimate load) at the respective mean cyclic load levels resulted in large increases in the displacement in a relatively few number of cycles. The rates of displacement were large and decreased to a minimum after which they rapidly increased to a peak value. The stiffness modulus showed lower initial values than in the low amplitude cases and degraded rapidly with increasing numbers of cycles. The skin friction reached a peak which progressively moved down the pile shaft during cyclic loading. When the peak reached the pile base the skin friction along the entire shaft decreased to a low residual value, which in turn caused the point resistance to increase continuously.

An increase in the mean cyclic load level in the low amplitude piles produced a slightly larger displacement at a specific number of cycles whereas for the high amplitudes an increase resulted in a reduced displacement. The mean cyclic load level appeared to have little effect on the degradation of the sand-pile system stiffness modulus. The skin friction was mobilised lower down the pile shaft for a larger mean cyclic load level.

An important finding was that, for all piles independent of the applied cyclic load, at a total pile head displacement of about 10% of the pile diameter, the skin friction at the pile base began to decrease while at the same time the rate of pile displacement started to increase. It was therefore concluded that at this displacement no or little skin friction remained along the pile shaft and the behaviour of the pile was fully controlled by the point bearing resistance.

The work presented in this report forms an important contribution to the research into the understanding of the behaviour of realistic piles due to cyclic loading. Future tests are required to expand and further support the observations, particularly if the cyclic parameters are altered.

TABLE OF CONTENTS

Acknowledgments i

Synopsis ii

Table of contents v

List of illustrations viii

1. INTRODUCTION AND OBJECTIVES 1

2. LITERATURE REVIEW 3

2.1 Cyclic Shear Tests on Sand 3

2.2 Cyclic Shear Tests of Sand-Concrete Interfaces 5

2.3 Cyclic Axial Load Tests on Piles in Sand 6

2.3.1 Pile types and installation methods 6
2.3.2 Loading Procedure 7
2.3.3 Pile response to cyclic loads 9

3. EXPERIMENTAL TEST PROGRAM 17

4. EXPERIMENTAL FACILITIES AND SOIL MATERIAL 20

4.1 Test Site and Apparatus 20

4.1.1 Test pit 20
4.1.2 Loading device 20
4.1.3 Pile driver 22

4.2 Sand Embedment for Piles 22

4.2.1 Sand properties 22
4.2.2 Sand placement and compaction 24

4.3 Pile Installation 27

4.3.1 Driving of pile casings 27
4.3.2 Pressure grouting 28

5. ELECTRONIC INSTRUMENTATION AND DATA CAPTURING 30

5.1 Load and Displacement Measurements 30

5.2 Strain Measurements 31

5.2.1 Attachment and connection of gauges 31
5.2.2 Strain calculation 36

5.3 Data Acquisition System and Program Control 38

6. OVERVIEW OF PROGRAM OF LOAD APPLICATIONS 41

7. TEST RESULTS AND DISCUSSION 44

7.1 Pile Geometry and Characteristics 44

7.2 External Characteristics of Pile Behaviour 47

7.2.1 Static load-displacement response 47
7.2.2 Displacement versus number of load cycles 50
7.2.3 Rate of displacement versus number of load cycles 56
7.2.4 Cyclic load-displacement response 62
7.2.5 Ultimate load capacity after cyclic loading 64

7.3 Internal Characteristics of Pile Behaviour 65

7.3.1 Load distribution along pile shaft 65
7.3.2 Skin friction distribution along pile shaft 67
7.3.3 Point resistance of piles 74
7.3.4 Analysis of hysteretic behaviour at pile tip 77

8. SUMMARY AND INTERPRETATION OF RESULTS 81

9. CONCLUSIONS 88

LIST OF REFERENCES 91

APPENDIX A 94

LIST OF ILLUSTRATIONS

FIGURES **PAGE**

2.1 Schematic diagram of cyclic load parameters 8
2.2 Displacement - number of cycles relationship (after Chan and Hanna, 1980) 10
2.3 Overall displacement - number of cycles relationship 11
(after Chan and Hanna, 1980)
2.4 Rate of pile head displacement - number of cycles relationship 11
(after Chan and Hanna, 1980)
2.5 Rate of displacement - number of cycles relationship 12
(after Hanna et al., 1978)
2.6 Mechanism of failure at the pile tip (after Touma and Reese, 1974) 16
4.1 Schematic of test pit and loading device 21
4.2 Particle size distribution of Cape Flats sand 23
4.3 Dry density - moisture content relationship of sand 24
4.4 Shear stress - normal stress relationship of sand 25
5.1 Position of strain gauges on reinforcing bars 32
5.2 Scanned image of photograph of mounted strain gauge and wiring 33
5.3 Schematic of gauge assembly 34
5.4 Scanned image of photograph of in-situ gauge assembly (with covering) within a . 34
grouted pile
5.5 Wheatstone bridge connection of strain gauges 35
5.6 Calibration curves for strain gauge positions on pile 43 38
6.1 Load - displacement relationship of pile 42 43
7.1 Load - displacement relationship of statically loaded piles 48
7.2 Load - displacement relationship of piles with MCLV of 30kN 49
7.3 Load - displacement relationship of piles with MCLV of 60kN 49
7.4 Load - displacement relationship of piles with MCLV of 90kN 49
7.5 Load - displacement relationship of piles with amplitude of 10kN 50
7.6 Load - displacement relationship of piles with amplitude of 30kN 50
7.7 Displacement envelope during the 2nd cyclic sequence of pile 42 51
7.8 Displacement - number of cycles relationship of piles with MCLV of 30kN 53
7.9 Displacement - number of cycles relationship of piles with MCLV of 60kN 53
7.10 Displacement - number of cycles relationship of piles with MCLV of 90kN 53
7.11 Displacement - number of cycles relationship of piles with amplitude 55
of 10kN
7.12 Displacement - number of cycles relationship of piles with amplitude 55
of 30kN
7.13a Displacement rate - number of cycles relationship of piles with MCLV 59
of 30kN
7.13b Displacement rate - number of cycles relationship of piles with MCLV 59
of 30kN (logarithmic scale)

FIGURES **PAGE**

7.14a Displacement rate - number of cycles relationship of piles with MCLV of 60kN 59
7.14b Displacement rate - number of cycles relationship of piles with MCLV of 60kN (logarithmic scale) 59
7.15a Displacement rate - number of cycles relationship of piles with MCLV of 90kN 59
7.15b Displacement rate - number of cycles relationship of piles with MCLV of 90kN (logarithmic scale) 59
7.16a Displacement rate - number of cycles relationship of piles with amplitude of 10kN 61
7.16b Displacement rate - number of cycles relationship of piles with amplitude of 10kN (logarithmic scale) 61
7.17a Displacement rate - number of cycles relationship of piles with amplitude of 30kN 61
7.17b Displacement rate - number of cycles relationship of piles with amplitude of 30kN (logarithmic scale) 61
7.18 Example of hysteresis loop with fitted regression line 63
7.19 Sand-pile system stiffness modulus - number of cycles relationship 63
7.20 Load - displacement relationship during determination of ultimate load capacity after cyclic loading 65
7.21 Load distribution along pile shafts at selected loads 67
7.22 Skin friction distribution along shaft of pile 42 (MCLV=30kN, Ampl.=10kN) . . 70
7.23 Skin friction distribution along shaft of pile 53 (MCLV=90kN, Ampl.=10kN) . . 70
7.24 Skin friction distribution along shaft of pile 43 (MCLV=30kN, Ampl.=30kN) . . 72
7.25 Skin friction distribution along shaft of pile 52 (MCLV=60kN, Ampl.=30kN) . . 72
7.26 Point load - number of cycles relationship of pile 53 (MCLV=90kN, Ampl.=10kN) 75
7.27 Point load - number of cycles relationship of pile 52 (MCLV=60kN, Ampl.=30kN) 75
7.28 Contact pressure - displacement relationship of steel plates at various depths within the sand mass (after Schwaeble, 1991) 76
7.29 Schematic of variables used in calculation of elastic compression of sand 79
8.1 Displacement - number of cycles relationship of all test piles 83
8.2 Rate of displacement - number of cycles relationship of all test piles (logarithmic scale) 85
A1 Scanned image of photograph of drop-weight pile driver 95
A2 Scanned image of photograph of piles in Series 3 96
A3 Scanned image of photograph of piles in Series 4 97
A4 Scanned image of photograph of piles in Series 5 98

TABLES **PAGE**

2.1 Type and dimensions of selected pile tests 7
4.1 Sand properties (Cowburn, 1990) 23
4.2 In-situ dry densities and moisture contents of each test series 26
6.1 Test program of piles 43
7.1 Dimensions of excavated piles 45
7.2 Compressive strengths of pile grouts and pile caps 46
7.3 Young's moduli of pile grouts 46
7.4 Displacement and number of cycles when point skin friction at pile tip drops 73
7.5 Point bearing and contact stresses at selected displacements 77
7.6 Calculation of elastic compression below pile tip at selected cycles 79

CHAPTER 1:
INTRODUCTION AND OBJECTIVES

For many years there has been considerable interest in the cyclic loading of soils and structural elements embedded in soils. Many foundations do not sustain a constant load, but are subjected to fluctuating loads. These cyclic loads are caused by various natural factors such as wind loading, thermal loading, wave loading, tidal fluctuations, traffic loading and changes in storage loads.

Concern regarding the effects of cyclic loading on the response of these foundations, especially piles, within the surrounding soil medium has been generated principally due to the fact that the interactions that take place between the soil and pile are highly complex and generally not fully understood. The need to study these interactions became apparent after it was realised that when a sample of soil or a structural foundation was loaded in cycles there was a change in the state of stress at the end of the load cycle compared to that at the beginning. Therefore as more load cycles are applied there is a progressive readjustment of the stress state along the shaft and hence a change in behaviour results. In nature a foundation can be subjected to a large number of load cycles during its life time and the cumulative effects thereof should be considered at the design stage.

Studies of the effects of cyclic loads on foundation structures have concentrated on the behaviour of piles and anchors. The study of piles has generally focused on piles used as foundations for offshore structures (eg. Bea, 1992; Lee and Poulos, 1991) and transmission towers. The research has been both experimental (eg. Chan and Hanna, 1980) and theoretical (eg. Poulos, 1989). However, there is a great need for more detailed experimental data as it is only against this data that theoretical studies can be validated. The majority of experimental investigations have concentrated on very small-scale laboratory tests. Although many full-scale tests have been undertaken, they have only considered static loading due to the immense difficulties in applying cyclic loads in the field.

The lack of experimental data on large scale piles initiated this research program to study the behaviour of pressure-grouted piles subjected to cyclic loads. The complex mechanisms of skin friction degradation that occur along the soil-pile interface are not well understood and therefore the major objective of the research was to investigate the skin friction using instrumented piles.

The research has been limited to an experimental study of grouted piles in a sand medium at natural moisture content. The investigation considers the influence of axial sinusoidal loads at a constant frequency of 0.25 Hz on the pile behaviour. A major objective is to study the effects of the mean cyclic load level and the load amplitude on the pile performance during cyclic loading. Specific attention will be given to the skin friction distributions along the pile shaft with increasing cycle numbers.
The analysis is limited as the objective of the work was to carefully collect experimental data in a systematic manner which will then form the basis of more detailed analyses during future work.

Initially the existing literature on cyclically, axially loaded piles in sand is presented. The experimental test program that was developed is then discussed, followed by a description of the experimental facilities, soil material and pile installation procedure. The electronic instrumentation and method of capturing the data is explained. The program of load applications is described in detail after which the test results are presented, discussed and interpreted. Finally some conclusions of the research work, based on the analysis of the data, are drawn.

CHAPTER 2:
LITERATURE REVIEW

Cyclic loading caused by natural phenomena can be either random or systematic. The most commonly occurring cyclic loads are non-dynamic and this research is therefore limited to the non-dynamic type. Non-dynamic loading occurs if the rate of loading is such that the inertial forces are insignificant when compared to the static forces.

The cyclic loads imposed axially on a pile cause an up and down movement of the pile shaft which in turn imparts a cyclic shear strain to the surrounding soil (Chan and Hanna, 1980). The behaviour of this soil-pile system is therefore a complex combination of the effects of the loading on the soil itself and on the system as a whole. In order to understand the processes involved during cyclic loading an attempt is made to subdivide the topic into the behaviour of cyclically loaded:

- soil as a material
- soil-concrete interfaces and
- structural elements (piles) in a soil embedment

Since the piles tested in this experimental investigation were installed in a sand material, the soil considered in this review will be limited to sand.

Each subject will be addressed in terms of the findings of various research papers which will provide explanations of the observations during pile testing. The review does not claim to be a complete study of all these aspects.

2.1 Cyclic Shear Tests on Sand

A sand that is subjected to cyclic shear exhibits dilatancy or densification. Both these situations are characterised by a highly non-linear stress-strain relationship (Cuellar et al., 1977). The degree to which these phenomena occur depends mainly on the relative density

a low relative density show a decrease in volume while those at a higher density undergo an increase in volume.

Little relative movement of the sand grains occurs at small strains and therefore the volume change is small. The stress-strain response of the sand will be largely linear and elastic and the hysteresis loops indicate little damping. At higher strains, however, the non-linearity of the stress-strain behaviour is more pronounced leading to lower values of shear moduli but higher values of damping (Silver and Seed, 1971a). The grain rearrangements result in the shear modulus increasing with increasing number of cycles and decreasing with increasing strain amplitude. Such rearrangements can occur either by crushing of the particles or by the particulate structure of the granular medium being sufficiently distorted to enable the particles to fall or slide past each other.

The rearrangement of the particles results in an increase in the density of dry sand as reported by Youd and Craven (1975). It was shown that when a sand was exposed to a wide range of cyclic shear strains of constant amplitude, while a constant normal stress was maintained, it experienced densification. Silver and Seed (1971b) produce similar findings and discovered that a greater densification was produced for larger shear strains.

Strain-controlled cyclic simple shear tests of Cuellar et al. (1977) indicate that the densification of sand subjected to cyclic shear and the shape of the hysteresis loops are strongly dependent on the strain amplitude, the total number of cycles, the confining stress and the relative density of the sand. The width-to-height ratio of the loops increases greatly with amplitude and decreases with number of cycles, while the loops become steeper with an increase in the number of cycles.

The conditions of the tests already mentioned differ from those conditions occurring in the sand adjacent to the pile shaft during cyclic loading. Andersen and Moussa (1973), as quoted by Chan and Hanna (1980), conducted shear tests in which the laboratory test conditions closely approximated the strain conditions on the soil adjacent to the pile shaft. The sand surrounding a pile shaft is subjected to cyclic shear stresses under approximately constant volume conditions. Cyclic shear stresses of constant amplitude (ie. stress-

controlled) were applied to the sand samples at a frequency of about 0.7 Hz. The sand volume was kept constant during the test by varying the normal stress. All the tests showed a progressive decrease in the normal stress until failure occurred. The drop in normal stress increased rapidly with an increase in the amplitude of the shear stress for a given number of cycles. It could therefore be reasoned that continuous cyclic loading of a pile may lead to a reduction in the normal stress surrounding the shaft at a certain stage during loading, thus resulting in a decrease in the side shear resistance (skin friction).

2.2 Cyclic Shear Tests of Sand-Concrete Interfaces

It is not clear which role the immediate contact zone between grout and sand plays in the load transfer mechanism acting along the pile shaft. However, numerous research publications deal with experimental and numerical investigations of the interactions at interfaces of various materials.

A limited number of interface tests, however, have been conducted to investigate the effects of changes in the soil type, shaft material, moisture content and density of the soil, grain size, contact pressure and the type and magnitude of the applied loading on the interface skin friction. Potyondy (1961) found that, in static tests, increases in both the soil density and the surface roughness caused an increase in the skin friction.

Desai et al. (1985) postulated an interface mechanism that occurs during cyclic loading based on tests of sand-concrete interfaces conducted in a translational test box. Previously it had been thought that the interface action was concentrated exactly at the interface. However, Desai et al. considered the idea that the interface action for many soil-structure interfaces, except possibly those in clays and smooth structures, occurred in a thin zone near the interface. It was observed that during cyclic loading, soils developed shear bands with slip surfaces. This could result in a thin, deforming soil layer separating the pile shaft and the soil. The material in this zone would experience an increase or decrease in density depending on the initial density and the soil type. In turn the interface would stiffen or soften during loading.

Desai et al. (1985) established that the peak or mobilised shear stress increased with number of cycles for both relative sand densities of 15% and 80%. The increase at a higher density was not as rapid as that for the lower density. The interface exhibited increased stiffness as the normal stress was increased. The maximum mobilised shear stresses due to cyclic loading are influenced notably by higher displacement amplitudes and rates.

2.3 Cyclic Axial Load Tests on Piles in Sand

From an overview of existing literature on the topic of cyclically loaded piles it became evident that all previous experimental data differed widely with respect to the methods employed for pile installation, the pile type and the loading procedures. These topics are therefore discussed separately after which the major findings in terms of the pile behaviour are presented.

2.3.1 Pile types and installation methods

A wide variety of research has been undertaken into the behaviour of numerous types of piles in soil. The materials most commonly used for pile shafts include timber, metallic sections including steel and aluminium, reinforced concrete and grout. The methods most frequently used in the installation of field test piles are driving (Appolonia and Romualdi, 1963; Lehane et al., 1993; Vesic, 1970) and bored, in-situ cast techniques (Reese et al., 1969). In laboratory tests, driven piles made of a metallic section are most commonly reported in the literature (eg. Chan and Hanna, 1980; Poulos, 1981a). The choice of a metal section was common for all instrumented piles as the strain response is more easily determined. The only data available for grouted piles was that in the work of Lee and Poulos (1991) and Koreck and Schwarz (1988).

A relatively large number of full-scale field tests are published. However, the applied loading was only static and hence, although these tests all lead to a general understanding of pile behaviour, they are not specific to the intended research and are therefore not considered in this review.

The majority of cyclically loaded pile tests published in the respective literature were conducted on small-scale laboratory piles. These are therefore concentrated on and the selected tests are listed in Table 2.1. The tests of Koreck and Schwarz (1988) were incomplete and hence the results are not discussed.

Table 2.1 : Type and dimensions of selected pile tests

Pile Type	Diameter (mm)	Length (mm)	Author
Aluminium, Driven, Instrumented	9	570	Chan and Hanna (1980)
Aluminium, Jacked	20	250	Poulos (1981a)
Aluminium/Grout, Instrumented	50	634	Lee and Poulos (1991)
Pressure Grouted	130	5000	Koreck and Schwarz (1988)

The tests reviewed are difficult to compare directly due to differences in the surrounding soil mediums, dimensions of the piles and the installation techniques. The effects that these variables have on the behaviour of the piles are not easily determined.

2.3.2 Loading procedure

Some terms need to be defined prior to the explanation of the loading schemes. A load can be applied to a pile under either stress- or strain-controlled conditions. The most commonly occurring natural loads are stress-controlled (eg. wave action). Also, in-situ field tests are almost exclusively stress controlled and therefore it was decided that this type of load control should be adopted in this research.

Stress-controlled cyclic loading can be applied in either one-way or two-way modes. In a one-way mode the load fluctuates either only in tension or only in compression, whereas in two-way mode the load alternates between tension and compression.

Cyclic loading comprises many variables. In the literature a wide variety of terms exist for one and the same variable. Therefore, a brief definition of terms used in this research is given and shown in Figure 2.1. The cyclic loading is applied about a Mean Cyclic Load LeVel (MCLV) at a certain amplitude (half of peak to peak). The frequency of loading and one such load cycle, of sinusoidal waveform, is clearly demonstrated in the figure.

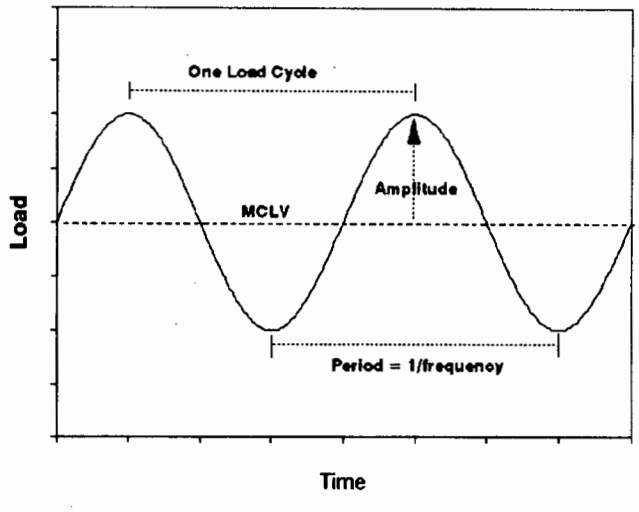

Figure 2.1 : Schematic diagram of cyclic load parameters

Since no recommendations on cyclic pile test procedures exist, a wide variety of loading techniques was found in the literature. It appears that most of the adopted procedures were arbitrary and controlled by their specified facilities in the laboratory.

Lee and Poulos (1991) present tests on instrumented, model, grouted piles in calcarious sand. The behaviour under both displacement- and load-controlled conditions was investigated. The load sequence applied under displacement control involved initially loading the pile statically to failure after which cyclic loading was applied, between predetermined limits of displacement, for a specified number of cycles. Failure was defined as a displacement of 10% of the pile diameter. Subsequently, the piles were again loaded to failure to determine the ultimate load capacity after cyclic loading.

The load-controlled tests began by loading the pile statically to a specified mean load (MCLV). Cyclic loading between predetermined limits of load for a specified number of cycles was then applied. The pile was finally loaded statically to failure.

Chan and Hanna (1980) conducted a series of pile tests using a variety of cyclic loading modes including compressive to zero, tensile to zero and compressive to tensile loads. Since the envisaged test program is to investigate only compressive loading the compressive scheme is therefore considered. The peak loads ranged from 10% to 50% of the ultimate capacity and the load was always reduced to zero during a load cycle. The frequency of loading was 0.017 Hz and the load was altered between the upper and lower limit in 7 seconds after which it was held constant for 23 seconds.

Although Poulos (1981a) investigated the behaviour of piles in clay and not sand, the test procedure employed is of interest. The piles were tested under two-way load-controlled cyclic loading. The load was applied at a frequency of about 0.5Hz. The tests involved initially statically loading the pile to failure. After a rest period the pile was then subjected to cyclic loading and finally loaded again statically to failure after cyclic loading had ceased.

Koreck and Schwarz (1988) conducted cyclic load tests using sinusoidal wave forms at frequencies of about 0.02Hz. The tests were load-controlled and the piles were tested under both one-way and two-way modes. Static load tests were also performed on specific piles to provide reference capacities for the cyclic tests.

2.3.3 Pile response to cyclic loads

Chan and Hanna (1980) show the response of a pile subjected to cyclic loading in terms of both the accumulated displacement of the pile head and the rate of displacement versus number of cycles. In their investigation the hysteretic load-displacement response of the pile head, as well as the load distribution and load transfer (skin friction) along the pile shaft, is analyzed. The pile movement, rate of

movement, axial shaft load and shaft friction for a specified number of cycles, refer to the values at the maximum load during the cycle.

An interesting observation worthy of a more detailed discussion is that during the initial stages of loading the results show that, in terms of the displacement versus number of cycles relationship, two distinct types of behaviour exist depending on the magnitude of the load. From Figure 2.2 it can be seen that the change in behaviour occurs between loads of 0.25 $Q_c/0$ and 0.30 $Q_c/0$, where Q_c is the ultimate load capacity. For cyclic loads larger than this, the total movement increased continuously after the first few cycles. The overall pile movements are shown in Figure 2.3.

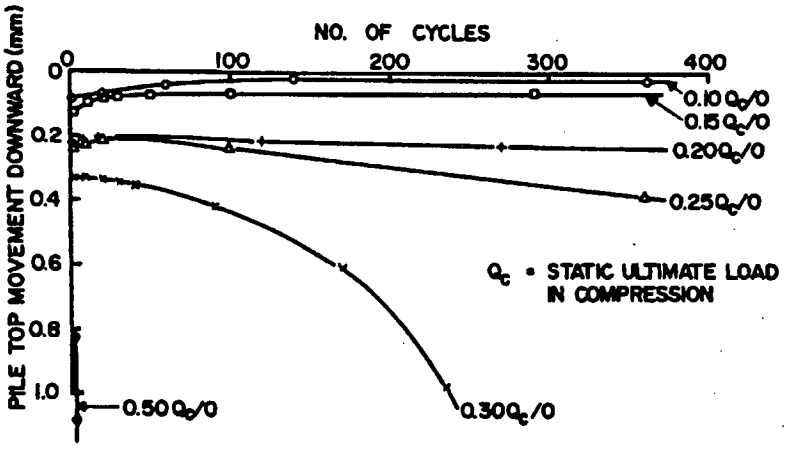

Figure 2.2 : Displacement - number of cycles relationship (after Chan and Hanna, 1980)

In terms of the rate of displacement per load cycle (see Figure 2.4), the principal effect of the cyclic loading in all cases was to bring about a change from an initial 'stable' stage with small rates of penetration to a relatively 'unstable' stage with large rates of displacement. The number of cycles which defined the stage of rising rates of displacement increased with decreasing load. The rising rate was followed by a sudden decrease in the rate of displacement. It was found that the response of a pile subjected to small amplitudes was characterised by a long period of a relatively 'stable' stage that extended over thousands of cycles.

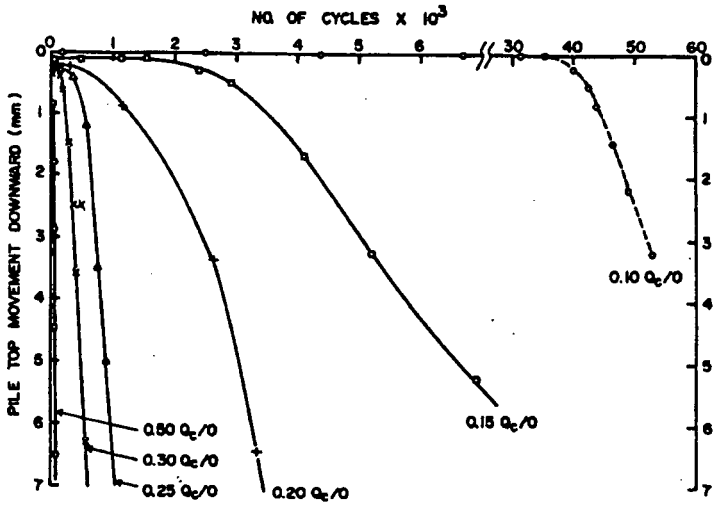

Figure 2.3 : Overall displacement - number of cycles relationship (after Chan and Hanna, 1980)

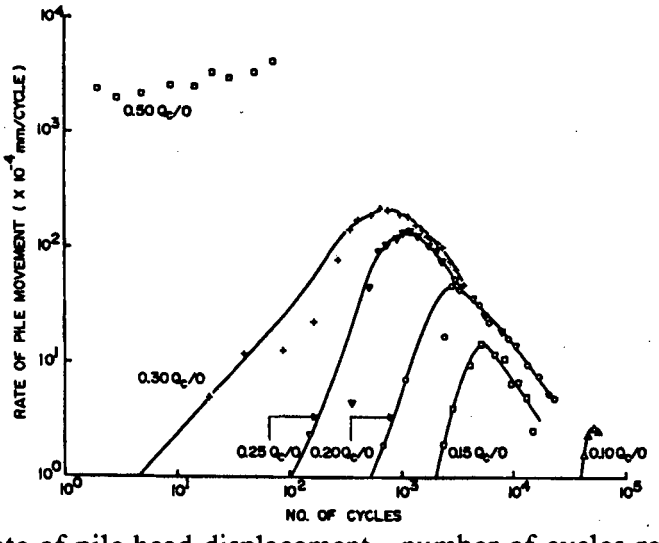

Figure 2.4 : Rate of pile head displacement - number of cycles relationship (after Chan and Hanna, 1980)

Work done by Hanna et al. (1978) on the behaviour of anchors subjected to repeated loads was investigated as it provides an insight into the mechanisms occurring at the soil-structure interface. The anchor response was presented in terms of the displacement versus the number of load cycles relationship in logarithmic scales. The results showed that the displacement of an anchor depends primarily on the load amplitude during cyclic loading in one-way mode. The higher the amplitude the fewer the number of cycles to cause 'failure'.

The rate of displacement versus the number of load cycles relationship is shown in logarithmic scale in Figure 2.5. Several stages in the rate of displacement can be seen

in the curves presented. An initial straight line relationship of decreasing rate, at various load levels, is followed by a change where the displacement increases per cycle. Finally the rate of displacement again decreases.

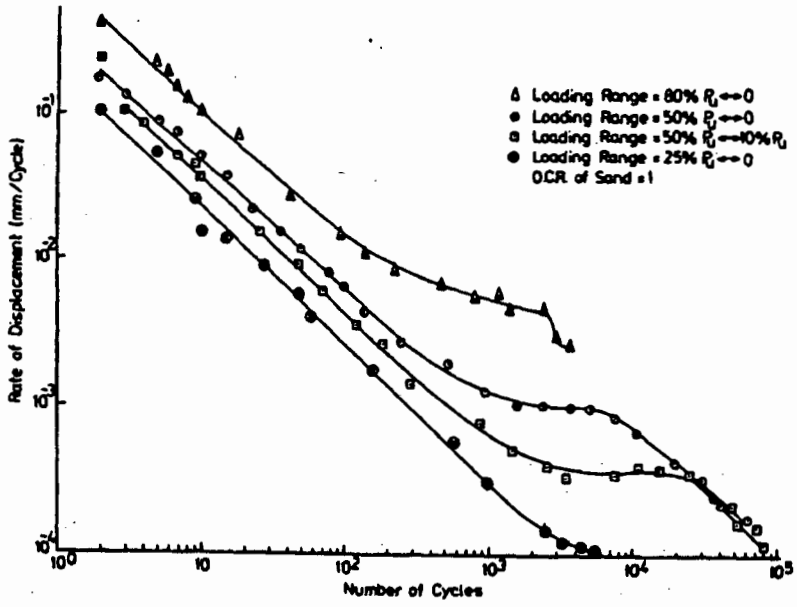

Figure 2.5 : Rate of displacement - number of cycles relationship (after Hanna et al., 1978)

Trochanis et al. (1987) investigate the hysteretic dissipation of piles under cyclic loading by way of a finite element analysis; however, it appears that the only experimental data on the hysteretic load-deformation response of a structural element in a soil is published by Hanna et al. (1978). It was observed that during the tests the area of the hysteresis loop in the load-deformation diagram became progressively smaller. After a few thousand cycles the loop reached an almost stable state. There was, however, a gradual build-up of very small permanent displacements. This was attributed to the fact that there was some grain slip accompanied by a breakdown of the grain corners. The stiffening effect was possibly due to an increase in density of the surrounding sand during cyclic loading. These observations are supported by the work of Youd (1972) who showed that additional densification of sand during repeated loading was due to crushing of individual particles.

Instrumented pile tests allow the determination of the load distribution along the pile shaft during cyclic loading. Two research papers, listed in Table 2.1, were

instrumented and therefore provided an insight into the complex interactions occurring along the sand-pile interface.

Before the actual stress distribution along the pile shaft (derived from strain gauge measurements) due to cyclic loading can be analyzed, the effect of residual stresses along the shaft and at the base should be considered. Most analyses assume an initially stress free pile although Poulos (1987) demonstrated that residual stresses could influence the behaviour of a pile. Residual stresses are more prevalent in driven piles than grouted piles due to the induced stresses during installation. The presence of initial residual stresses during cyclic loading has two effects. Firstly, the shaft capacity is reduced because reverse slip, and therefore cyclic degradation, is initiated more rapidly. Secondly, the cyclic pile head stiffness is reduced when compared to a case of no initial residual stresses existing along the pile shaft (Poulos, 1987). The influence of the residual stresses becomes less important as the number of cycles increases. The effect is most severe for relatively small cyclic load levels and small numbers of cycles.

After casting a pile the concrete (grout) changes in volume due to shrinkage and temperature changes (Touma and Reese, 1974). These volumetric strains can result in relative displacements of points on the pile in a vertical direction which may produce load transfer and hence residual stresses.

The cyclic degradation of a pile in sand can be observed in the breakdown of skin friction along the pile shaft (Scheele et al., 1991). Appolonia and Romualdi (1963) describe the mechanism of failure in piles as follows: as load is applied, the soil adjacent to the pile distorts. A nearly linear relationship between applied load and load transferred would exist as long as the soil was bonded to the pile along its entire length. A loading is reached at which the soil begins to slip along the pile and the shearing resistance will then reach a maximum. The zone of shear failure begins at the top of the pile shaft and progressively moves downwards with increasing load. When the ultimate shearing strength is reached at the bottom of the pile any further increase in load must be carried by the tip.

Poulos (1981b) supports the observation of a progressive movement of shear failure down the pile shaft. The small model pile tests demonstrated that cyclic degradation began at the pile top and progressed downward as the cyclic load (amplitude) or the number of cycles increased. The ultimate load capacity and cyclic stiffness decreased with increasing number of cycles and increasing cyclic load level (amplitude). The effect of the number of cycles on the pile behaviour became more significant when the cyclic load level approached 50% of the ultimate static capacity. Relatively little reduction in ultimate load capacity occurred for cyclic load levels less than 50% of the ultimate static value. However, for cyclic load levels in excess of about 55% failure was more than likely to occur. As the cyclic load level increased the degradation of both the ultimate skin friction and the soil modulus became pronounced, particularly near the pile top. This led to more load being carried in the lower part of the pile.

A crucial factor in determining the amount of cyclic degradation is the critical shear strain for skin friction. An increased amplitude imparts a larger shear strain to the soil which would accelerate the degradation.

The instrumented tests of Lee and Poulos (1991) indicate that the skin friction degradation under displacement-controlled loading depends on the magnitude of cyclic displacement and more specifically the cyclic slip displacement which is defined as the difference between the overall cyclic displacement and the displacement required to develop a full slip at the interface. The slip displacement is found to be between 0.5% and 1.5% of the pile diameter.

The strain gauge measurements showed that the load carried at any position along the pile decreased with increasing number of cycles as a result of the degradation of the shaft resistance.

The results of the load-controlled tests showed that if the cyclic load level (amplitude) did not exceed 20% of the static load capacity, cyclic loading had no effect on the axial capacity of the pile. Under one-way loading 600 cycles of load from 0% to 55%

of ultimate load caused failure. It was concluded that the load transfer characteristics were affected by the combinations of the MCLV, amplitude and the number of load cycles.

Chan and Hanna (1980) examined the changes in the base load and shaft friction as a result of repeated loading. As the rate of pile movement increased the base load also increased. During the stages of large rates of displacement there were substantial reductions in shaft friction - up to 83% reduction in the middle part of the shaft. A possible explanation was that the repeated loading caused a decrease in the lateral soil pressure on the pile as a result of the breakdown in grain size of the sand.

The base load provides the major resistance to the applied load after the skin friction has degraded. The mechanism of failure at the pile tip is discussed by Touma and Reese (1974). The high pressure at the tip is believed to cause arching of the sand around the tip. The downward movement of the pile causes two zones to develop around the tip - the flow zone and the arching zone (see Figure 2.6). The arching causes an increase in the stresses in the non-yielding sand near the tip. The sand then flows towards the pile near the tip to replace the subsiding sand. Above the flow zone there is an increase in the horizontal stresses at the pile wall. This can occur anywhere between 0 and 5 times the pile diameter above the tip.

From the above review it can be concluded that the behaviour of a pile subjected to cyclic loading is the result of a highly complex interaction process and is dependant on many factors, the most important being the mean cyclic load level, the amplitude of load and the number of load cycles. It was found that an increase in the number of cycles in low amplitude tests brought about a change in behaviour from an initially stable stage with small rates of displacements to an unstable stage with larger rates. The cyclic stiffness decreased with an increase in the number of cycles. Small amplitudes had very little effect on the pile behaviour. Higher amplitudes caused high displacements, even possibly failure. In general, the failure of a pile can be determined from either an increase in the permanent displacement to an unacceptable limit (about 10% of the pile diameter) or from the degradation of skin friction.

During cyclic loading there is a progressive redistribution and degradation of skin friction from the top to the bottom of the pile until the point resistance becomes prominent.

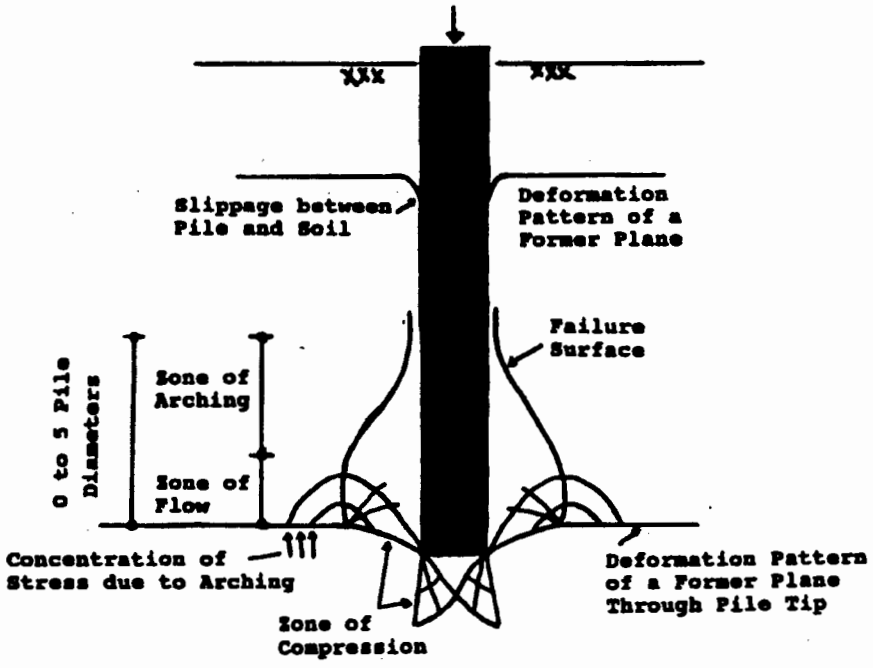

Figure 2.6 : Mechanism of failure at the pile tip (after Touma and Reese, 1974)

The response of a pile can be investigated by examining many aspects such as the load-deformation response, the rate of displacement, the accumulation of permanent displacement of the pile head and the load transfer along the pile shaft in terms of the skin friction and point resistance.

The results of the research to follow will attempt to clarify the behaviour of pressure-grouted piles in sand.

CHAPTER 3:
EXPERIMENTAL TEST PROGRAM

The test program that forms the basis of this research was developed after the review of existing literature on the topic of cyclically, axially loaded piles.

It was established that the majority of experimental research in this field has involved the testing of small-scale model piles under highly idealised conditions. While these contribute significantly to the understanding of the processes involved during cyclic loading, it was felt that larger scale in-situ pile tests in the laboratory would lead to more realistic and useful data which could then be closely related to field piles. With this in mind it was decided to initiate a laboratory test program using methods of pile installation that are actually employed in the field.

Pressure-grouted piles were decided upon as they are frequently installed as foundations for offshore structures (Lee and Poulos, 1991). The installation methods are also well suited to the confines of the laboratory.

Most previous research has concentrated on the external response of piles due to cyclic loading. However, to understand the interactions occurring at various levels along the pile shaft, instrumented pile tests are required. The literature review highlights the fact that very few large-scale, axially and cyclically loaded, instrumented pile tests have been performed on piles. Notably, no such tests exist for pressure-grouted piles. It was therefore decided that instrumented pile tests should form one of the main objectives of this research program.

In many other published experiments sand has been widely used as the medium into which piles were installed and it was therefore decided that a locally available Cape Flats sand should be used in this research. This sand is in abundance and is therefore economically

viable. It was shown (Cowburn, 1990) that careful preparation of this sand could provide a homogeneous embedment of a constant density. This was important as comparisons between a large number of piles would be required. The mechanisms involved during cyclic loading of sand samples have also been well established (as presented in chapter 2). Sand, of different origins and properties, is common in offshore conditions where the effects of cyclic loading on piles are of the utmost importance.

The behaviour of piles in sand not only depends on the soil characteristics, but also on other variables related to the installation and the loading procedures of the piles. Those due to the installation technique include the length and the diameter which is a function of the grout pressures and the sand density. The variables associated with the pile loading are the mode (one-way or two-way) and control of loading (ie. displacement- or load-controlled), the rate of load application during static loading, the waveform, frequency, amplitude, MCLV and the number of cycles during cyclic loading. Therefore, in order to obtain repeatable experimental results the preparation of the sand bedding, the installation of the piles and the applied loading were required to be well controlled.

Existing work, as presented in chapter 2, has mostly concentrated on the performance of piles subjected to a loading where during each cycle the load was reduced to zero. In those cases when the load level was increased both the MCLV and the amplitude changed. The individual effects of the MCLV and the amplitude on the pile performance could therefore not be determined. Since the response of piles to cyclic loading is a function of the combination of MCLV and amplitude, it was decided that the primary objective of the research would be to try and establish the individual effects of these two parameters on the interaction of piles in the sand. The test program was therefore developed to study the effects of these two variables by changing only one parameter at a time. To provide a reference level for the MCLV and the amplitude, in terms of the ultimate load capacity of the piles, it was decided to determine this capacity during static loading tests.

Since one-way stress-controlled loading closely approximates the natural conditions of loading that field piles are subjected to, it was decided that this form of loading should be

employed in the tests. The loading is also the most widely used and hence direct comparisons with existing data would be possible.

Although natural loading patterns are often random, sinusoidal wave forms best represent the loading patterns created by wind, wave and tidal action. The wave form is easy to apply using a function generator and for these reasons a sinusoidal waveform was chosen.

A frequency of loading of 0.25Hz was selected as it is similar to that produced by rapid wave loading (Head, 1986) and traffic loading of bridge abutments (Rosmanith, 1993). This frequency would also enable the application of a large number of cycles in a reasonable time limit.

An initial two series (series 1 and 2) of piles were tested in a provisional program (Cowburn, 1990) to establish ultimate loads, displacements and the effects of load amplitudes at various MCLVs on the response of piles in sand. This provided the knowledge and experience required to produce accurate experimental results during the following test program (series 3 to 5) which is described in this report.

The performance of the piles will be investigated in terms of the load and displacement response as well as the load transfer characteristics along the pile shaft.

CHAPTER 4:
EXPERIMENTAL FACILITIES AND SOIL MATERIAL

The laboratory was especially equipped for the installation and testing of pressure-grouted piles in sand. A prerequisite was a large test pit in which the sand could be placed and the piles installed. A sophisticated loading device was allocated particularly for these tests and a special pile casing driver was developed in the departmental workshop.

4.1 Test Site and Apparatus

4.1.1 Test pit

The laboratory test pit had the dimensions 6.0m * 1.6m * 3.0m. The side walls and floor consisted of heavily reinforced concrete in order to provide complete rigidity, thereby preventing lateral relaxation of the compacted sand during testing. The dimensions of the test pit permitted the installation of a maximum of four piles during a specific test series. A schematic of the test pit in elevation and cross-section is shown in Figure 4.1.

4.1.2 Loading device

Horizontal rails positioned on top of the side walls of the test pit enabled the attachment and exact positioning of a loading bridge above the pile heads. A structural frame mounted on the loading bridge housed the servo-controlled actuator and a load cell. The actuator and the load cell were laid out for a capacity of 200kN, in either tension or compression. A 22kW hydraulic power pack supplied the actuator. The layout of the loading system is also shown schematically in Figure 4.1.

Since continuous test periods of a few weeks were envisaged a water cooling system was installed to keep the oil temperature constant. An electronic, relay-operated temperature gauge was fitted to the oil sump to monitor the operating temperature.

The servo-valve, mounted on top of the loading actuator, was controlled via an electronic controller. The pile test system makes use of closed loop control circuitry. This control unit was described in detail earlier (Scheele et al., 1991).

The controller allowed any option to load the piles :

- load- or displacement-controlled
- static or cyclic
- sinusoidal, triangular or rectangular wave forms
- one-way or two-way loading
- amplitudes to a maximum of $\pm$ 200kN
- frequencies in the range of 0 to 2Hz

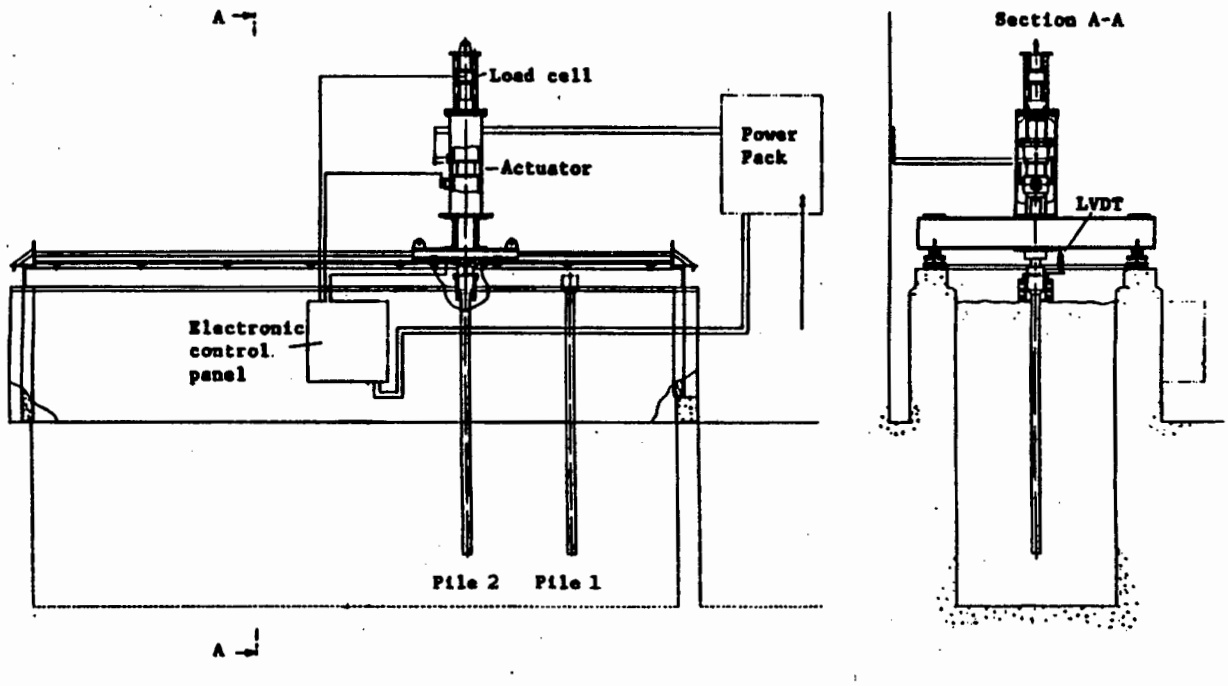

Figure 4.1 : Schematic of test pit and loading device

4.1.3 Pile driver

A specially designed pile driver was manufactured to enable precision driving of the steel casings into the sand embedment. It consisted of a 113kg drop weight which had a constant drop height of 700mm. The weight was lifted by a hydraulic piston and automatically released. The casings were driven to the required depth as a result of the impact on a special cap mounted on top of the casing. A scanned image of the pile driver is shown in Figure A1 in Appendix A.

4.2 Sand Embedment for Piles

A uniform and homogeneous sand embedment was required in all test series throughout the test program. To achieve this the compaction specific properties of the sand were determined and, in trial tests, an optimum method of sand placement and compaction was developed.

4.2.1 Sand properties

The soil was a uniform, round-grained, clean quartz sand that originated from the Cape Flats. Numerous tests were undertaken to determine the physical and chemical properties of the sand.

The particle size distribution of the sand was determined according to BS1377:Part2 (1990). The grading curve (see Figure 4.2) shows a uniformly graded medium sand. The coefficients of uniformity and curvature are 2.00 and 1.02, respectively.

The following properties shown in Table 4.1, were determined in independent research studies (Cowburn, 1990).

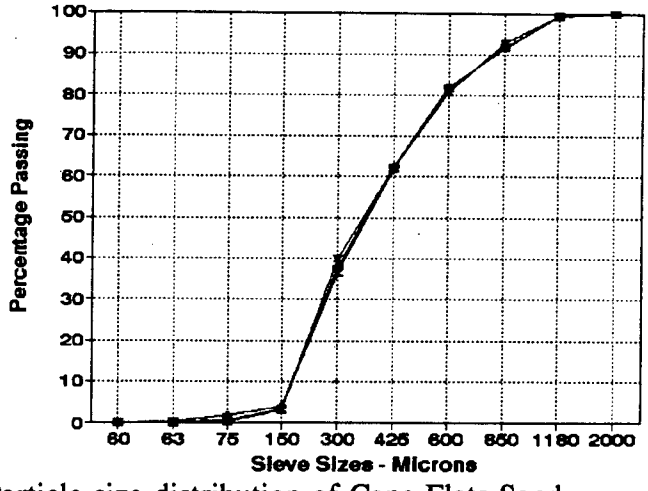

Figure 4.2 : Particle size distribution of Cape Flats Sand

Table 4.1 : Sand properties (Cowburn, 1990)

Relative Density	2.6
Natural Moisture Content (after 1 year of standing in the laboratory)	3.1%
Minimum Dry Density (dry test)	1487 kg/m^3
Maximum Dry Density (dry test)	1765 kg/m^3

Compaction tests were carried out to determine the dry density - moisture content relationship (ASTM D698 - Method A, 1987). In Figure 4.3 two curves are shown, which indicate two density peaks at various moisture contents. The maximum dry density of 1690 kg/m^3 is achieved at an optimum moisture content of 13.4%.

The average carbonate content of the sand was established as 17.8% using the method according to ASTM D4373-84 (1987). Higher values would result in a sand that is more susceptible to crushing during compaction.

In shear box tests it was established that the internal angle of friction ranged from $\phi = 28°$ to 39° as a function of the density (Scheele et al., 1991). These tests, however, were performed on dry sand samples. Since the shear strength of a sand depends on the density and moisture content (Head, 1982), extra shear box tests were

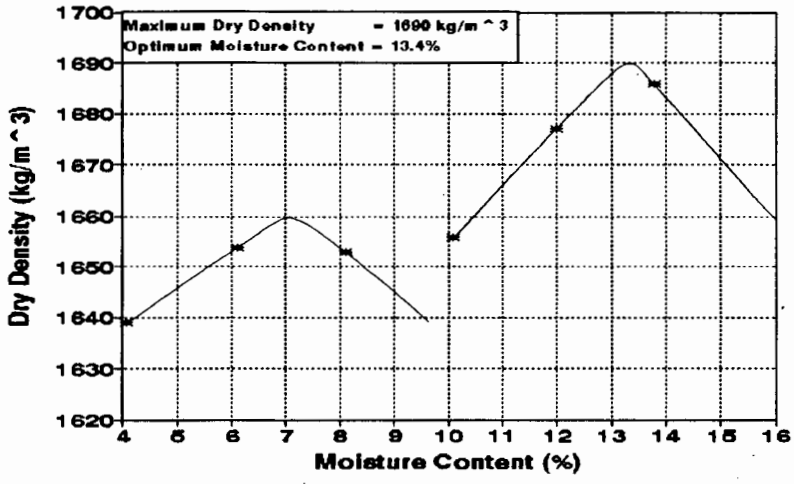

Figure 4.3 : Dry density - moisture content relationship of sand

conducted to determine the shearing properties of the sand at moisture contents and densities similar to those experienced in the test pit during testing. The target dry density and moisture content was therefore 1565 kg/m^3 and 4.2%, respectively (see section 4.2.2). The normal stresses applied to the samples varied from 11.0kN/m^2 to 39.7kN/m^2 which were approximately equivalent to the vertical stresses at depths of 0.7m to 2.5m below the test pit surface.

The results in Figure 4.4 show the friction angle to be about $\phi = 41°$ at an average dry density and moisture content of 1547kg/m^3 and 3.8%, respectively. It is assumed that this is the maximum friction angle occurring in the test pit during testing conditions.

4.2.2 Sand placement and compaction

In order to enable direct comparisons of the behaviour of piles from different test series a soil bed of repeatable uniformity, homogeneity and density was required. The placement and compaction procedure used in previous work led to a very controllable and uniform soil mass (Cowburn, 1990; Schwaeble, 1991) and was therefore applied in this research.

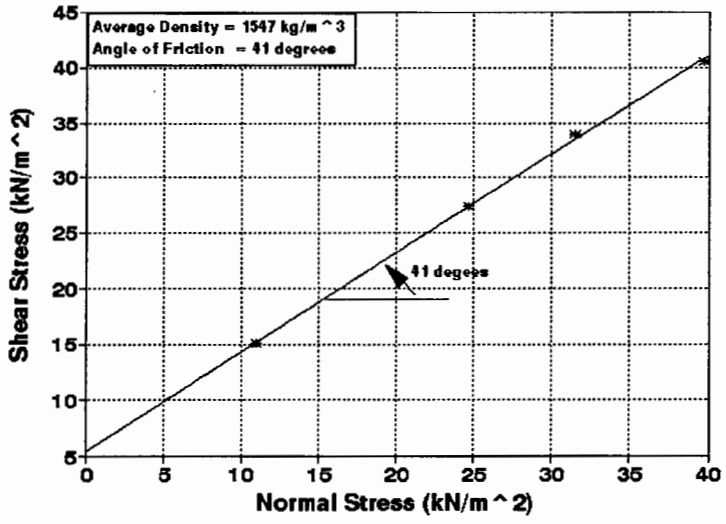

Figure 4.4 : Shear stress - normal stress relationship of sand

There was, however, some uncertainty prior to the commencement of the third test series about the number of passes of the Vibromax 1900 plate compactor that were required to achieve optimum compaction. An investigation was therefore instigated (Schwaeble, 1991) to determine the optimum number of passes. It was established that four passes were in fact best to achieve optimum compaction. A nuclear density testing device was used to correlate the in-situ densities and moisture contents. The results of Schwaeble (1991) confirmed the uniformity and repeatability of both the densities and moisture contents.

Briefly, the method of soil placement and compaction involved the placement of sand in layers of 300mm in the test pit at moisture contents as close to optimum as possible. The layer was then compacted with four passes of the compactor in accordance with the method given by Cowburn (1990). The in-situ bulk and dry densities were then determined after the compaction of each layer. The results of the average values for each test series are presented in Table 4.2.

It is evident that the in-situ densities and moisture contents of each layer immeadiatly after compaction were uniform. These moisture contents were about 8.6% which is below the optimum of 13.4%. It was observed that the soil drains exceptionally quickly and hence during compaction the moisture migrated from the top of the layer

to lower levels. It can therefore be assumed that the actual moisture contents prior to compaction were higher ie. closer to the optimum.

Table 4.2 : In-situ dry densities and moisture contents of each test series

Test Series	In-Situ Dry Densities		Moisture Content after Compaction		Moisture Content at Excavation
	Average (kg/m^3)	Std. Dev. (σ)	Average (%)	Std Dev (σ)	Average (%)
3	1563.10	16.4	8.8	0.8	4.19
4	1567.00	22.1	8.3	1.6	4.55
5	1563.80	17.0	8.8	0.6	3.75
Ave.	1564.63	18.5	8.63	1.0	4.16

A loss in moisture from the compaction to excavation stages is evident. The excess pore water drained to the bottom of the test pit to such an extent that after one day a significant water table appeared in the pit. This occurred during test series 3 and therefore, for subsequent series, a simple drainage system was installed in order to remove the water table.

The drains consisted of PVC pipes (ϕ_{ext}=90mm) drilled with 4mm diameter holes and covered with a geofabric (Bidim) to prevent the ingress of sand particles. Water was then drained out of the pipes via thin tubes once the entire pit was filled with sand. This method proved to be highly effective and allowed all excess water to be removed prior to the installation of the piles.

The average Young's modulus of the compacted sand, derived from cone penetrometer test results, was approximately 18.8GPa (Cowburn, 1990).

4.3 Pile Installation

The installation of the pressure grouted piles involved two stages - the driving of steel casings into the sand and pressure grouting.

4.3.1 Driving of pile casings

Installation of the piles commenced with the driving of an open-ended steel casing of 76mm diameter (internal) into the compacted sand. The casings were driven into the sand to the required depth using the drop weight pile driver (discussed in section 4.1.3). The sand was then augured from inside the casing using a hand auger. Care was taken not to auger below the tip of the casing.

The required depth was 2.4m in test series 3. However, after analysis of the results it was decided to decrease the pile length to 2.2m for series 4 and 5 to ensure that the ultimate capacity was well within the range of the actuator's loading capacity.

The pile length was chosen so as to give the longest possible length without the test pit boundaries affecting the stresses developed during loading. A maximum length of about 2.5m was suggested by finite element studies undertaken earlier by Bradley (1988). The studies, however, consisted of a simple static analysis of a 76mm diameter pile loaded in the test pit up to 80kN. The material was characterised by a variety of constitutive models.

During series 3 a water table of 1.41m was present in the test pit. As the drainage system was not present at that stage, water was gradually withdrawn from inside the casings until the water level had been lowered enough to allow removal of the sand from inside. However, the water in casing 2 was lowered too quickly and it was noticed that sand flowed into the casing - it was assumed that piping had occurred and that there would be an enlarged cavity just below the casing. It was then decided to remove the sand from the casings beneath the water level using a high-vacuum pump. The results were very satisfactory.

4.3.2 Pressure grouting

The test piles were cast in-situ using the method of compaction or pressure grouting. A brief explanation of the processes involved follows : a cement/water mixture (grout) is injected into the pile casing under high pressures. The sand surrounding the point of injection is densified in a radial direction through compaction as the grout mass expands under pressure.

The exact diameter of the resulting grouted pile is affected by the surrounding soil properties, density, moisture content and the grout injection rate and pressure (Warner, 1978).

The principal controlling factor in compaction grouting is the applied grout pressure which is usually monitored at the grout pump and the injection point. The area for greatest control is to ensure that the rate of pressure increase is not too rapid. The maximum allowable rate should be 35-40 kN/m^2 per minute (Rodio, 1989).

Prior to grouting a single Y16 reinforcing bar, with wire centralisers attached to the top and bottom, was inserted into the casing. Uplift of the sand during grouting was sometimes noticed in the trial run series which lead to a non-uniform grout column near the surface. Heavy sand bags were therefore placed on the sand surface around the casings in order to prevent up-lift of the sand near the pile top.

The grouting procedure was carried out with the assistance of a geotechnical contractor. The equipment consisted of a 250 CFM air compressor which supplied the required pressures, a grout mixer and a piston-type grout pump. The high pressure grout hoses were attached to the top of the casing using a special pressure cap. The pressure cap was fitted with a pressure gauge and a release valve which were both used to manually control the pressures in the casing during actual grouting. A special bracket was fastened to the casing below the pressure cap. This bracket had attachments to which an electric overhead crane was connected, thereby enabling the casings to be extracted. The grout in all series consisted of rapid hardening cement

with a water/cement ratio of 0.5. The grout was pumped into the casings at pressures of around 500kPa whilst the casings were continuously extracted. Near the surface (1m) the pressures were reduced to between 200kPa and 300kPa. Pressure was released 200mm from the surface to prevent bursting of the grout.

The pressures were difficult to maintain and for a few piles pressures exceeded the target of 500kPa. Generally, however, the pressures were well controlled.

The reinforcing bar of three piles (43, 51 and 54) pulled out partially with the casings during grouting. In piles 51 and 54 the reinforcing lifted by 1.3m. The bars were then hammered back into the unset grout column to ensure that the entire pile was reinforced. The total pull out of the reinforcing bar in pile 43 was 318mm. No correction was undertaken since the bar was instrumented. It was discovered that pull-out of the bar could be prevented by initially extracting the casing by 50mm before grout was injected into it.

After the grouting was completed the reinforcing bar protruded from the grout column. A pile cap was then cast onto the top of the pile a day after grouting. The cap provided the horizontal loading surface for the actuator. The pile caps were made in two ways. The cap of one instrumented pile in each test series was cast into a special steel mould that was later bolted directly to the piston of the load actuator. The strain gauge cables were pulled through small holes, drilled into the mid-section of the steel mould, before the cap was cast.

The other three pile caps in the series were cast into 150mm diameter tin cans. All pile caps were reinforced with the Y16 reinforcing bar protruding from the pile column as well as an additional cylindrical steel mesh. They were cast with a 0.35 water/cement ratio grout. The caps at the top of the excavated piles are shown in Figures A2 to A4 in Appendix A.

CHAPTER 5:
ELECTRONIC INSTRUMENTATION AND DATA CAPTURING

The applied load, displacement of the pile head and the strains along the pile shaft were monitored during the pile tests. The electronic instruments employed in order to undertake measurements included a load cell, linear variable displacement transducers, linear potentiometers and strain gauges which were connected to a computerised data acquisition system.

5.1 Load and Displacement Measurements

The 200kN load cell, situated at the top of the load actuator (as shown in Figure 4.1), was connected to the electronic control unit. The calibration constants were double checked in a separate calibration test and were found to closely agree with those supplied by the manufacturers.

The displacement of the pile head was recorded using either linear variable displacement transducers (LVDTs) or linear potentiometers (linpots). These electronic measuring devices were calibrated using a micrometer (0.01mm resolution) placed in a special calibration unit. The LVDTs were used for three piles (No. 31, 32 and 34) in series 3 after which it became apparent that a non-linear response was obtained near the extreme ranges of travel. The linpots were therefore used for the subsequent tests.

Axial loading of the piles required the accurate alignment of the load piston with the pile axis. It was noted that, in practice, the introduction of a small moment at the pile head could not be prevented. It was for this reason that two linear potentiometers were placed near the sides of the pile head at exactly opposite locations with respect to the pile axis. The linpots were aligned vertically and positioned an equal distance away from the pile

axis. They were fixed securely to a rigid support system that was external to the loading frame.

The devices were all supplied with the appropriate voltages by means of power supply units of high stability.

5.2 Strain Measurements

A major objective of this research was to record strain measurements along the pile shaft using strain gauges attached to the pile reinforcing. These measurements were necessary in order to investigate the load transfer characteristics at any stage of loading. This exercise required extremely accurate and careful preparation of the measuring points and data recording equipment of high accuracy.

5.2.1 Attachment and connection of gauges

a) Gauge attachment

The total number of strain measuring points along the pile reinforcing was limited to four due to practical considerations of cabling. The large amount of cabling had to be housed inside the casing during grouting while still allowing the grout to pass through.

Figure 5.1 shows the chosen positions of the gauges relative to the reinforcing bar for both pile lengths of 2.2m and 2.4m. The lowest gauge was placed slightly away from the bottom of the pile to ensure that a consistent grout body, without any sand inclusions or irregularities, would form around it. This was necessary as it had been noticed during previous work (Cowburn, 1990) that the tip often showed minor inconsistencies.

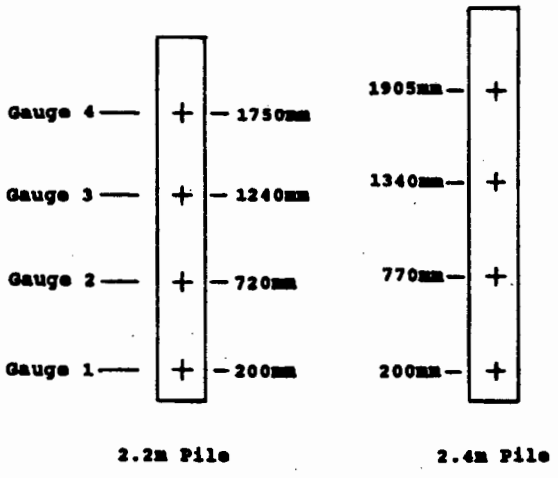

Figure 5.1 : Position of strain gauges on reinforcing bars

The selected strain gauges were 120 ohm Kyowa KFC-5-C1-11 gauges. They were 10mm long, 3mm wide, bonded foil gauges with gauge factors of 2.10. The gauges were temperature compensated for steel.

The limited surface area of the reinforcing bar restricted the number of attached gauges at each measuring position to two. The reinforcing bar was precisely machined at the gauge positions to form two parallel, 6mm wide and 50mm long flat surfaces on exactly opposite sides thus providing the area for adhering the two active strain gauges.

The entire area surrounding the surfaces was thoroughly cleaned and the surfaces themselves were finely sand-papered and washed with acetone. The gauges were aligned in the axial direction and mounted exactly opposite each other using a cyano-acrylate based strain gauge cement (Kyowa CC-33A). Soldering points were later glued next to the gauges to provide a connection point for the gauge lead wires and the cabling. The cabling was a 4 core, shielded cable with a 5mm diameter. Figure 5.2 shows a scanned image of a photograph of one of these connections.

Great care had to be taken to provide the protection and moisture proofing necessary to withstand the pressurised grouting conditions during installation. The gauges and soldering points were therefore covered with an initial 1mm to 2mm layer of butyl

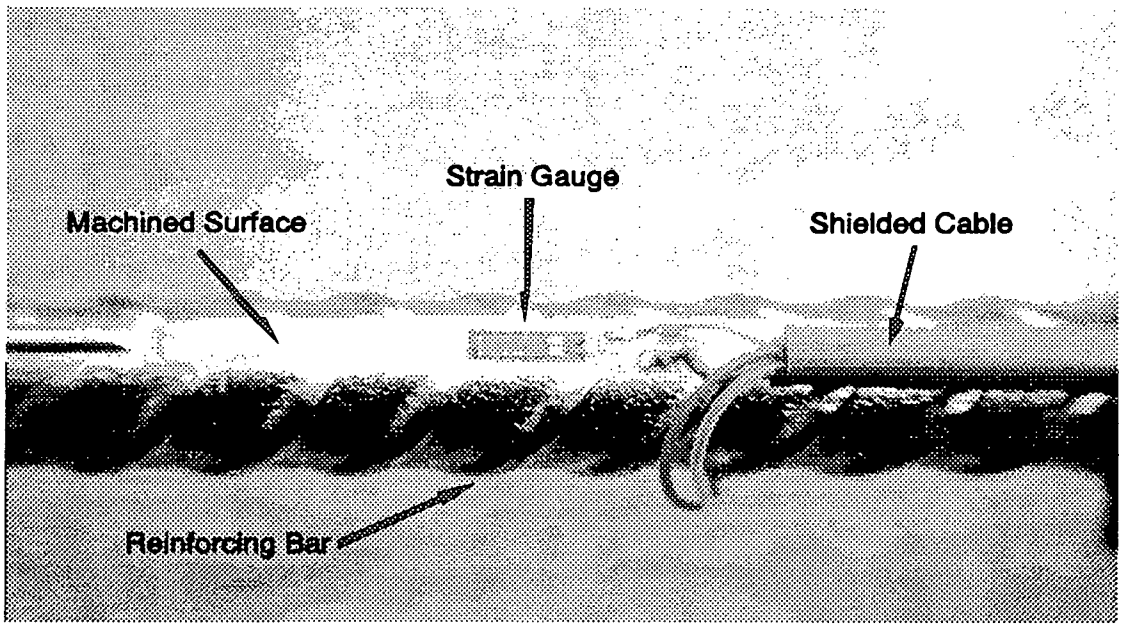

Figure 5.2 : Scanned image of photograph of mounted strain gauge and wiring

rubber (Kyowa C5). This also served as an insulator for the thin gauge lead wires. The entire installation was then covered with a 5mm layer of rubber-mixed-clay (AK22) which is ideally suited for moisture proofing at high pressures. The schematic of a gauge assembly is shown in Figure 5.3. An actual gauge assembly (with covering) within an excavated grouted pile is shown in the scanned image of a photograph in Figure 5.4.

In order to achieve accurate and reliable strain measurements the gauge insolation resistance must be above 500MΩ (Hewlett Packard, 1981; Kyowa, 1985). In all cases there was absolutely no contact of the gauges with the reinforcing implying an infinitely high resistance.

The cabling was attached along the whole length of the reinforcing bar with wire spacers. The excess cabling, required to reach the data acquisition equipment, was wound in tight bundles to minimise the area taken up during grouting. The cables for all the four gauge positions were exactly the same length to cancel the effects of differential thermal expansion of the wires.

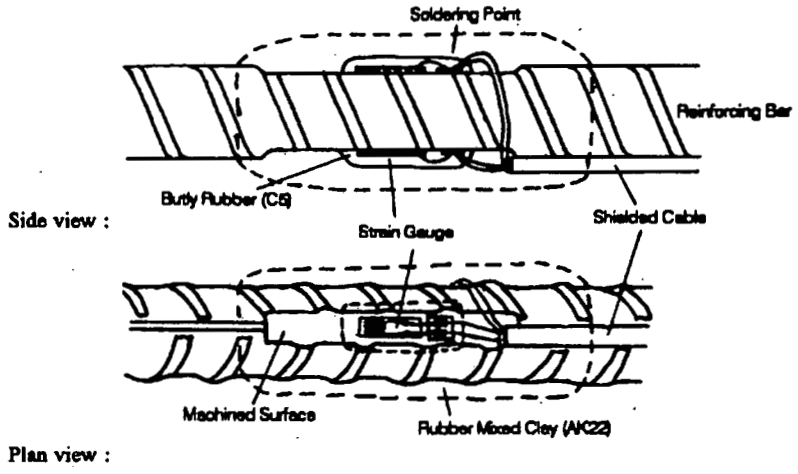

Figure 5.3 : Schematic of gauge assembly

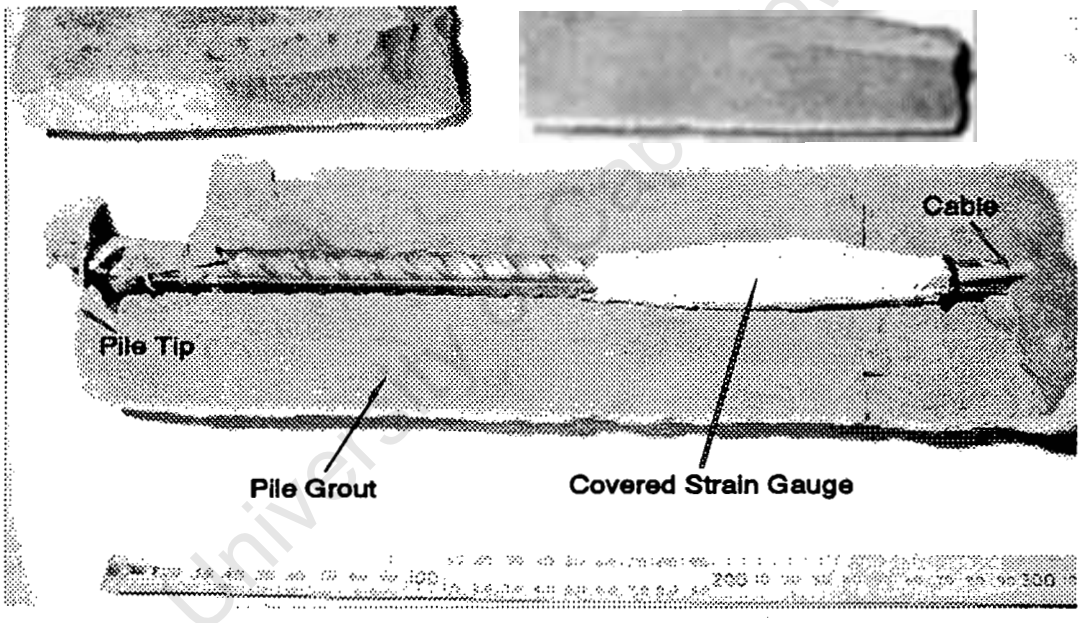

Figure 5.4 : Scanned image of photograph of in-situ gauge assembly (with covering) within a grouted pile

b) Gauge connection

The four strain measurement locations (consisting of two strain gauges each) along the reinforcing bar had to be connected in four separate Wheatstone bridges. The Wheatstone bridge circuit, shown in Figure 5.5, is the most frequently used circuitry for strain measurements due to its high sensitivity. A Wheatstone circuit used for

strain measurement is always a full bridge which can be either completely or partially formed by the active gauges on the test specimen.

Since only two active gauges could be used at each measuring position on the reinforcing bar, the bridge circuit could be completed using two fixed resistors inside the data acquisition system. However, in order to reduce the effects of temperature changes in these fixed resistors and hence obtain more accurate measurements, two external dummy gauges were used to complete the bridge. The dummy gauges were placed on separate short specimens of the same reinforcing bar and the lengths of the cables were the same as those of the active gauges. After careful waterproofing they were buried in the sand bed nearby the piles to ensure that their temperatures were as similar as possible to those of the active gauges. The method of attaching and covering the dummy strain gauges was exactly the same as that discussed for the active gauges.

The circuit configuration chosen is shown in Figure 5.5 where gauges R_2 and R_4 are active and R_1 and R_3 are passive (dummy). This arrangement results in a factor of amplification of two for the axial strain output and eliminates the effects of bending moments in the specimen.

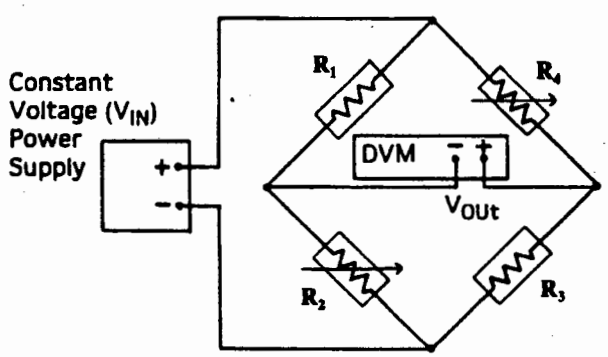

Figure 5.5 : Wheatstone bridge connection of strain gauges

5.2.2 Strain calculation

The strain at the position of the strain gauges can be determined either from first principles or from calibrations of the gauges. Both methods were employed and the results are compared.

a) Strain from first principles

The relation between an applied strain and the relative resistance change of a strain gauge is given by the equation :

$$\frac{\Delta R_g}{R_g} = GF * \epsilon \qquad (1)$$

where R_g = initial gauge resistance

ΔR_g = change in resistance

GF = gauge factor

ϵ = applied strain

The gauge factor is experimentally determined and supplied by the strain gauge manufacturers (GF = 2.1 in this case). The equation for strain in a full bridge circuit, as derived by Hewlett Packard (1982), is :

$$\epsilon = \frac{-2 V_r}{GF\ [\ (\nu+1) - V_r\ (\nu-1)\ ]} \qquad (2)$$

where

$$V_r = \left(\frac{V_{out}}{V_{ex}}\right)_{strained} - \left(\frac{V_{out}}{V_{ex}}\right)_{unstrained} \qquad (3)$$

and GF = gauge factor

ν = Poisson ratio

V_{out} = output voltage of bridge

V_{ex} = excitation (input) voltage

If R_1 and R_3 are dummy gauges then $\nu = 0$ and therefore Equation 2 becomes :

$$\epsilon = \frac{-2V_r}{GF\ [\ 1 + V_r\ ]} \qquad (4)$$

The axial strain at any gauge position can then be easily calculated using Equations 3 and 4. It should be noted that this equation holds for an unbalanced bridge and therefore there is no need for bridge balancing in this application. Any shifts in the supply voltage were not significant as the actual supply voltage was read before the strain gauges were scanned. A shifted value could then be inserted in equation 3. Throughout the test series there was, however, a maximum shift of only 0.5 milli-volts.

b) Strain from calibration

The instrumented reinforcing bars were tested and calibrated in tension to determine the quality and consistency of the signal response of the gauge assemblies. Poor alignment of the two gauges was therefore prevented by checking all gauges during calibration and replacing them if necessary. The gauges on the reinforcing were connected, together with the dummy gauges, to form the full Wheatstone bridge.

The relationship between load and output voltage of all the gauge positions was highly linear. Figure 5.6 presents a sample calibration test with both loading and unloading curves for each gauge position on the reinforcing bar of pile 43. The maximum tensile load applied was only 20kN.

The force at the gauge positions can be calculated using the calibration constants and the strains are then determined as follows :

$$\epsilon = \frac{F_{steel}}{E_{steel} * A_{steel}}$$

where F_{steel} = force applied to steel

A_{steel} = area of steel

E_{steel} = Young's modulus of steel

The exact cross-sectional area at the gauge positions was determined by machining two of the parallel surfaces along a 300.0mm section of reinforcing. This section was then weighed and the precise area was determined based on the steel density.

The strains were calculated at all gauge positions using both calibration methods and the values obtained differed by less than 0.2%. It was therefore decided to use the formulae during the actual analysis of the pile. The Young's modulus of the steel reinforcing bar was determined from these calibration curves. Its value was 205GPa which falls exactly in the range given in the specifications from the steel manufactures. The gauges were therefore assumed to be very reliable.

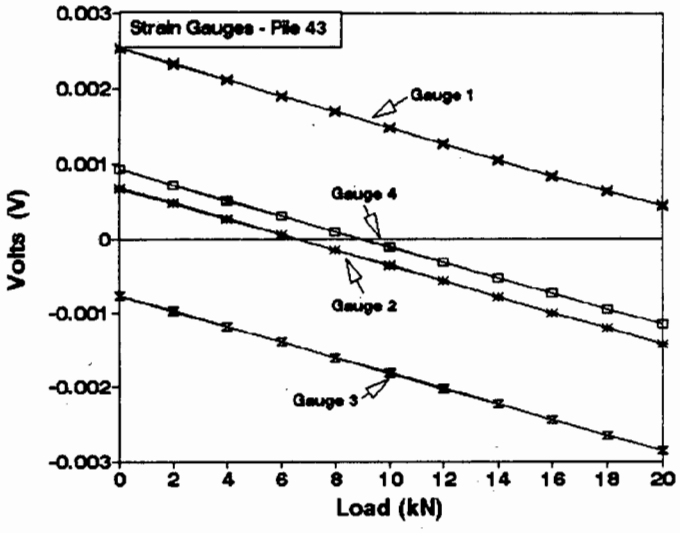

Figure 5.6 : Calibration curves for strain gauge positions on pile 43

5.3 Data Acquisition System and Program Control

The electronic instruments (linpots, load cell and strain gauges) output varying voltage signals in response to changes in displacement, load or strain. These signals were recorded and stored for later analysis. Sophisticated and relatively fast data acquisition equipment was therefore required. This system, consisting of a personal computer (PC) and a Hewlett Packard Data Acquisition/Control Unit, is discussed below.

The electronic instrumentation was connected with the Hewlett Packard 3497A Data Acquisition/Control Unit (data logger). The data logger was interfaced to an IBM

compatible PC via an HP-IB interface card. The PC acted as the system controller which was responsible for data acquisition, control, communication and data processing. On command from the PC the data logger received, as inputs, the voltage outputs from the system censors (load cell, linpots or LVDTs, strain gauges and power supplies) and sent those measurements over the communications interface (HP-IB interface) to the PC. This data was then stored on the PC hard disk. The control was provided by an operations program written in the C+ language.

The data logger had several expandable options which enhanced the acquisition facilities. The options used during this work included the following :

- a digital voltameter (DVM) which was a high quality, 5½ digit, 1 microvolt sensitive direct current (DC) voltameter ideally suited to measuring the low level outputs of strain gauges as well as the higher level outputs of the load cells and linpots (or LVDTs).
- a 20 channel relay multiplexer assembly which can be used to switch signals from up to 20 channels to the data logger. It was well suited for precise low level measurements.
- a 120 Ω strain gauge/bridge completion assembly which allowed the determination of strain of bonded resistance strain gauges by measuring voltage changes which occurred between the unstrained and the strained state of the gauge. This assembly provides bridge completion for strain gauges and any mixture of ¼, ½ or full bridges. The assembly required an external power supply for bridge excitation.

A highly stabilised power supply was used and the supply voltage was 4V. The bridge excitation voltage was always supplied, never switched, so there were no errors due to dynamic heating and cooling of the transducer. The supply voltage was measured on each assembly and therefore measurement accuracy was independent of long term power supply changes.

An XY chart recorder was connected to the load and displacement recording instruments to provide an analog display of the load-displacement response during any stage of loading. It

also served as a backup in the event of a fault occurring in the PC data capturing. An oscilloscope was available to check the exact frequency of loading.

As already mentioned, the data capturing was controlled by an application program designed and coded in C+. Data could either be captured continuously or at specified intervals. During cyclic loading continuous data capturing would have resulted in massive amounts of data that would not have been possible to store on hard disk. An option therefore existed to specify time intervals, in seconds, during which the program did or did not store data.

It was decided that during all pile tests a continuous batch of 16 seconds (4 load cycles) would be read every 400 seconds (100 load cycles) during cyclic loading. These intervals were, however, changed from time to time during the course of the test depending on the rate of pile movement.

The program analyzed data during idle times and if significant changes (as specified by the user) appeared on a specified channel, continuous reading and storage was initiated to ensure that this action was recorded.

Actual data was stored in original form (ie voltage readings). It was stored in files on hard disk in binary format to minimise file sizes. Another application program was run to convert the binary files into ASCI format which were then readable by Quattro Pro (Borland, 1992), the spreadsheet used for data analysis. All voltage readings were only then converted into actual loads and displacements using the respective calibration constants.

The maximum scan rate achieved for piles without strain gauges was 21 readings per second which is equivalent to 28 scans of all the instruments per load cycle. During tests on the instrumented piles only 12 scans of all instruments could be taken during each load cycle.

CHAPTER 6:
OVERVIEW OF PROGRAM OF LOAD APPLICATIONS

In chapter 3 the rationale for the decisions of the choice of the sand material, pile type and installation technique, mode and control of cyclic loading and the envisaged objectives of the loading program, was given. It is informative to present an overview of the actual program of load applications prior to the presentation of the results in the next chapter.

The program of the research work involved two kinds of tests :

Static tests : In order to provide a reference level for the choice of MCLV and amplitude it was necessary to establish the ultimate load capacity of the piles of a particular length during static load tests. The piles were loaded at an approximate rate of 40kN per minute until the pile displacements increased rapidly without any further increase in load. No other load rate was investigated.

Cyclic tests : Cyclic load tests with a variety of combinations of MCLVs and amplitudes were systematically followed to research the various pile responses. Three stages of loading were common to all cyclic load tests :

- Static loading at an approximate rate of 40kN per minute to a predetermined load
- Cyclic loading with a set amplitude about this predetermined load (MCLV)
- Static unloading and reloading to the ultimate load capacity of the pile.

The three load stages succeeded each other without significant interruption with respect to time.

In total, the test program consisted of the installation and load testing of 12 piles - three test series (3,4 and 5) of four piles each. The tests included two static tests to ultimate load, one instrumented 'quasi-static' test with three load cycles about each of three successive MCLVs and nine cyclic tests at different MCLVs and amplitudes. Four of the cyclically loaded piles were instrumented with strain gauges.

In Table 6.1 the respective loading characteristics with the envisaged length of each pile are listed. Some test results, namely the number of load cycles per cyclic sequence and the total displacement of the pile head (relative to the unloaded state) at the end of each sequence, are listed. These results are presented to provide a brief overview of the experienced magnitudes of displacements and the number of load cycles, as they have implications with respect to the pile responses.

It should be noted that the double digit pile number reflects the series (first digit) and the number of the pile in that series (second digit).

The piles are presented in order of increasing MCLV. For three of the low amplitude (10kN) piles, after the cyclic loading was completed, a second sequence of loading was applied at an amplitude of 20kN. This was done at the end of the proposed test to gain additional information which might have contributed to the understanding of the failure mechanisms and thereby enable the constant revision of the test program. An example of a complete load testing procedure, showing the various loading stages, is clearly demonstrated in Figure 6.1. Here the load-displacement relationship of pile 42 is plotted. The final loading to failure at the end of the second load sequence is illustrated in the insert (note the different scales). In general, this pattern of loading was followed throughout the cyclic tests. The various stages can be easily identified.

Both cyclic sequences are displayed in Table 6.1. However, only the test results of sequence 1 are presented, discussed and analyzed in the subsequent chapters as the comparison of sequence 2 with other piles is not always possible due to the prior loading history (ie. sequence 1).

Table 6.1 : Test program of piles

Pile No.	Mean Cyclic Load Level (kN)	Amplitude (1st Seq.) (2nd Seq.) (kN)	Total No. Cycles (1st Seq.) (2nd Seq.)	Displ. at end of cycles (1st Seq.) (2nd Seq.) (mm)	Length (mm)	Instrumented (Yes/No)
31	Static Test	-	-	-	2 400	N
41	Static Test	-	-	-	2 200	N
42	30	10 20	108 000 290 000	1.6 33.3	2 200	Y
43	30	30	45 000	66.1	2 400	Y
34	30	30	25 000	48.0	2 400	N
44	60	10 20	108 000 170 000	3.4 30.0	2 200	N
51	60	20	171 000	9.3	2 200	N
52	60	30	72 000	41.9	2 200	Y
53	90	10 20	108 000 100 000	4.96 16.6	2 200	Y
32	90	30	30 000	37.5	2 400	N
54	120	10	63 000	5.3	2 200	N
33	30,90,150 'quasi-static'	30	3 static cycles at each MCLV	68.0	2 400	Y

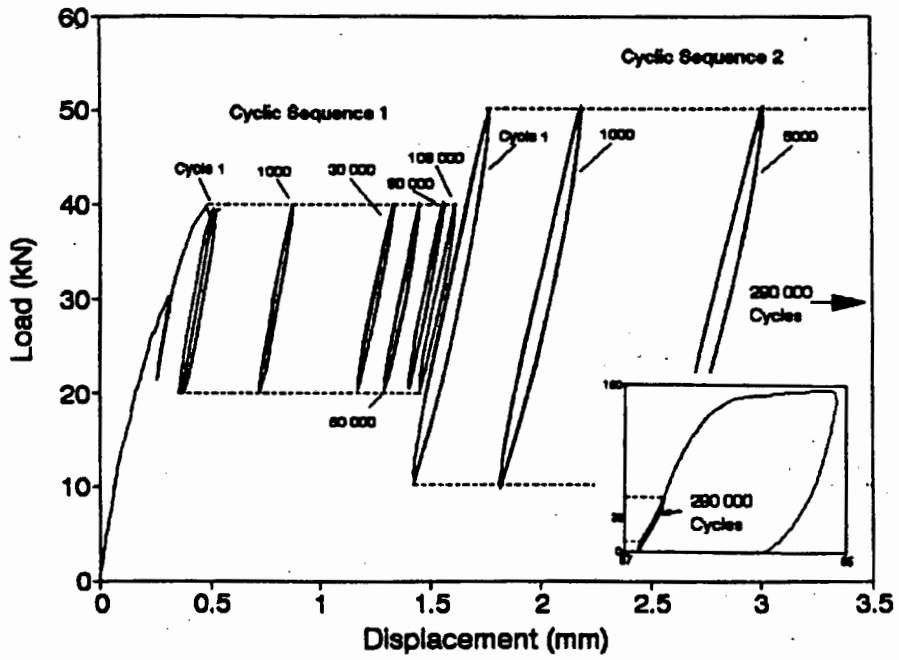

Figure 6.1 : Load - displacement relationship of pile 42

CHAPTER 7:
TEST RESULTS AND DISCUSSION

The performance of the piles was analyzed and grouped into external and internal behavioural characteristics. The external characteristics consist of the load-displacement response of the pile head during static and cyclic loading, the cumulative pile deformation, the rate of displacement of the pile head and the ultimate pile capacity after cyclic loading. Internal characteristics are defined as the distribution of load transfer along the pile during load application and redistribution of load transfer along the pile in terms of skin friction and base resistance with increasing number of cycles during cyclic loading.

Comparative studies of these external and internal considerations can produce practical and sensible results if the actual shapes (diameter and length) of the piles, determined after completion of the load test and their subsequent excavation, are taken into account.

7.1 Pile Geometry and Characteristics

The measurements of the excavated pile shafts are listed in Table 7.1. The diameters are quoted as average values of measurements taken at 200mm intervals along the pile shafts. The similarity of the average diameters and the small standard deviations thereof reflect the uniformity of the pile shafts. This confirms that a good degree of control was maintained during the grouting process. The uniformity of the pile shafts is also evident from the scanned images of the photographs of the excavated piles of series 3, 4 and 5 presented in Figures A2 to A4 in Appendix A. The pile diameters are larger than the external diameter (89mm) of the pile casings. This enlargement is due to the grouting pressures and varies between 9.4% and 17.6%. The pile lengths differ somewhat from the planned values shown in Table 6.1, due to limitations in the control of installations which are generally experienced in the field. Only two piles showed irregularities in shape; pile 32 displayed an

abnormal bulb-like tip which was a result of the hydraulic piping which occurred in the casing during auguring (see section 4.3.1).

Table 7.1 : Dimensions of excavated piles

Pile No.	Average Diameter (mm)	Std. Deviation (mm)	Diameter of tip (mm)	Length of Pile (mm)	Comments (measurements relate to pile tip)
31	100.1	1.5	97.3	2 340	very uniform, slight bulge near 2200mm
32	100.8	0.9	125.0	2 300	very uniform, very enlarged tip (bulb)
33	99.6	1.5	99.5	2 230	uniform, slight enlarged tip
34	99.6	2.2	95.5	2 340	very uniform, relatively smooth
41	100.7	3.6	94.5	2 025	uniform, rounded tip
42	98.1	0.9	96.8	2 100	very uniform, rounded tip
43	97.4	4.3	broke off	2 348	pronounced tapering shaft, lower 770mm broke off, very smooth over lower 1100mm
44	101.8	3.6	95.2	2 020	slight taper, uniform, thick near top
51	104.7	3.9	110.5	2 100	slightly enlarged tip, thick crust of sand on shaft, ave 110-114mm ϕ before crust removed
52	99.7	2.5	95.4	2 040	very uniform shaft
53	101.0	2.3	96.7	2 100	uniform, rounded tip
54	102.1	2.8	102.4	2 040	thick sand crust on shaft, uniform for bottom 1 000mm

Pile 43 has a tapered appearance and a low average diameter over the lowest 1m. This, together with the smooth nature of the pile shaft, suggests that the grout pressures were lower than those maintained during all the other pile installations. The reinforcing bar of this pile lifted during grouting and it was discovered during excavation that the un-reinforced lower portion of the pile had broken off during testing. The overall diameters of piles 51 and 54 are somewhat larger than the rest.

Examination of the strain gauges after excavation of the piles showed that the moisture proofing was effective.

The compressive strength of the pile grout and pile caps was tested prior to the commencement of a loading test. The tests were performed on 100mm cubes according to BS1881:Part 116 (1983). The results are listed in Table 7.2.

Table 7.2 : Compressive strengths of pile grouts and pile caps

Series No.	Average Compressive Strength of Pile Grout (MPa)	Average Compressive Strength of Pile Cap (MPa)	Sample Age (days)
3	25.3	72.2	12
3	38.7	-	35
4	46.7	76.9	30
4	55.1	-	49
5	29.5	73.4	36

The compressive strength of the grout in series 4 is somewhat higher than that in series 3 and 5. This may be due to a slightly lower water/cement ratio of the grout. The cube specimens may not be exactly representative of the actual pile grout as the conditions of casting differed. The cubes were vibrated while the pile was cast under pressure. Curing was similar in both cases as the cubes were buried in the test pit sand.

The Young's modulus of the pile grout was determined in each test series according to BS1881:Part 121 (1983). The moduli, listed in Table 7.3, were required in the analysis of the strain readings.

Table 7.3 : Young's moduli of pile grouts

Series No.	Ave. Young's Modulus (GPa)	Std. Deviation (σ)	Specimen Age (days)
3	14 (estimated)	-	-
4	15.27	0.09	49
5	10.34	0.28	36

7.2 External Characteristics of Pile Behaviour

The most basic information obtained from a pile load test is the load and displacement at the pile head. These measurements are plotted against each other in load-displacement diagrams. The engineer is familiar with these graphs in order to derive the ultimate loads or serviceability criterion for a particular situation.

7.2.1 Static load-displacement response

The exercise of the static loading tests was to determine the ultimate static capacity of the piles in the sand of defined density and moisture content. This served as a reference in the selection of appropriate cyclic load specifications in terms of MCLV and amplitude.

All the load-displacement curves of the statically loaded piles are shown in Figure 7.1. The load scale is limited to 200kN since this was the maximum load that could be applied. However, the ultimate capacities of piles 31 and 41 could not be obtained due to the limitation of the loading device. By extrapolating the respective load-displacement curves the ultimate capacities were estimated as 240kN and 210kN based on a widely accepted graphical method developed by Van der Veen (1953). The ultimate loads of piles 11 and 12 (Cowburn, 1990) were determined to be 190kN and 200kN, respectively. Their lower capacities may be attributed to the different patterns in loading. Piles 11 and 12 were loaded in cycles according to loading practices of grouted anchors (Code of Practice, 1989).

The first load step of the load-displacement response of pile 41 was not recorded due to a temporary malfunction of the load cell.

To allow comparisons of the initial static load-displacement responses of the other piles during static loading to the respective MCLVs, the pile responses are grouped into the categories of equal MCLVs (Figs. 7.2 to 7.4) or equal amplitudes (Figs. 7.5 and 7.6). The displacements in these figures are limited to 4mm thus showing only

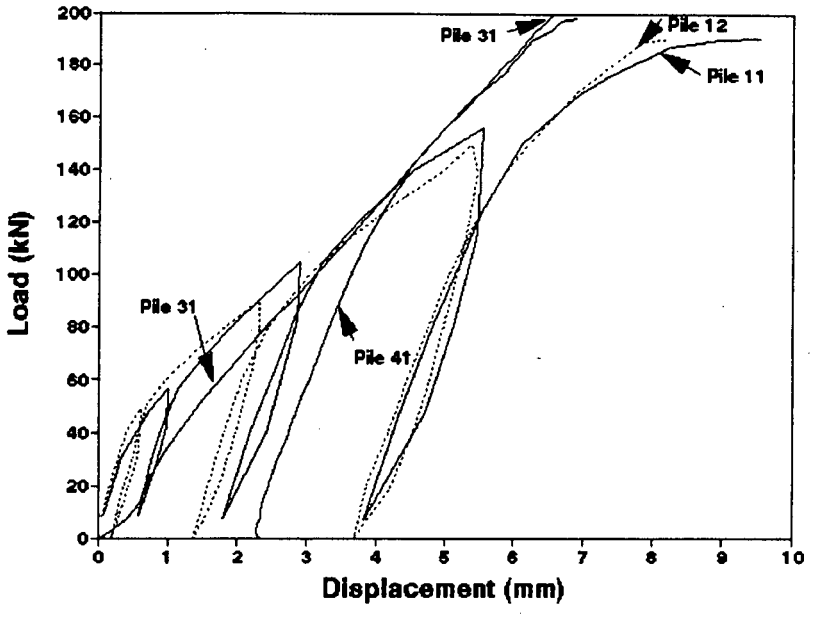

Figure 7.1 : Load - displacement relationship of statically loaded piles

the initial static loading curves followed by the first few load cycles at their MCLV and amplitude. Generally, the load-displacement responses of the piles in each category during static loading are in good agreement.

For a few piles the anomalies or deviations in geometry of the actual pile from an even cylindrical shaft are clearly reflected in the load-displacement behaviours. Pile 32 (Figures 7.4 and 7.6) has a bulb at the tip, pile 43 (Figure 7.2) has a small diameter and a very smooth tapering shaft and piles 51 (Figure 7.3) and 54 (Figure 7.5) have large diameters. Since piles 34 and 43 have the same loading pattern and pile 43 shows irregular static behaviour, the analysis will concentrate, where possible, on the results of pile 34 in preference to pile 43.

However, despite these few differences in behaviour the piles generally show very similar and repeatable initial static and cyclic load responses. It can therefore be noted that the experimental technique of this research work was highly controlled and that comparisons of different piles is therefore justified.

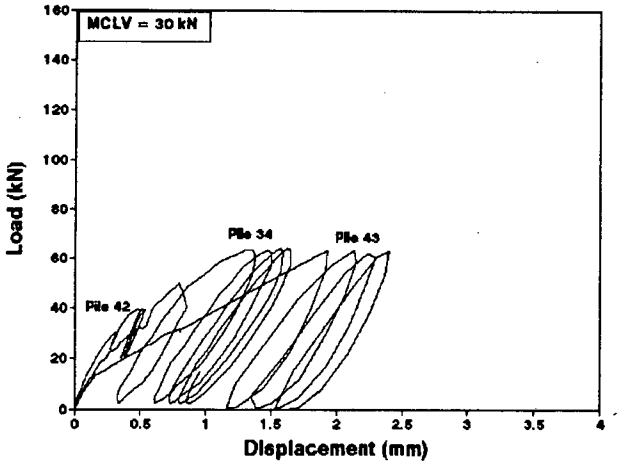

Figure 7.2 : Load - displacement relationship of piles with MCLV of 30kN

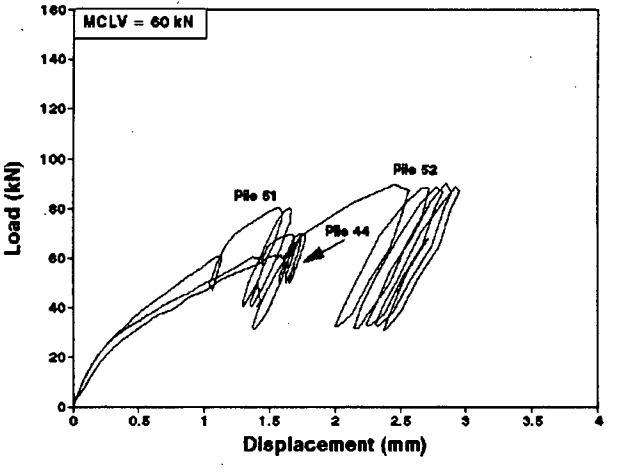

Figure 7.3 : Load - displacement relationship of piles with MCLV of 60kN

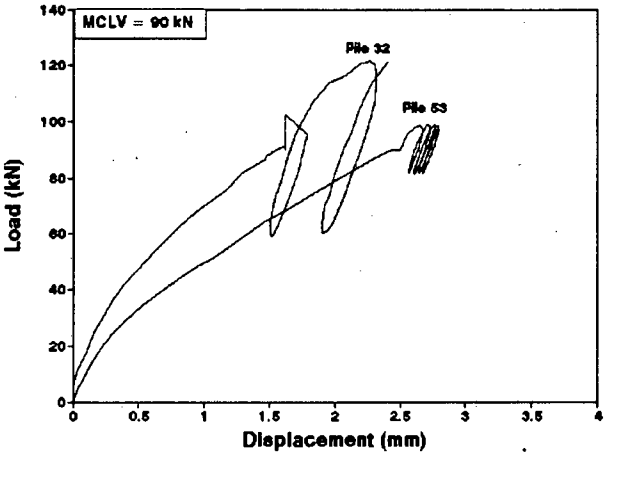

Figure 7.4 : Load - displacement relationship of piles with MCLV of 90kN

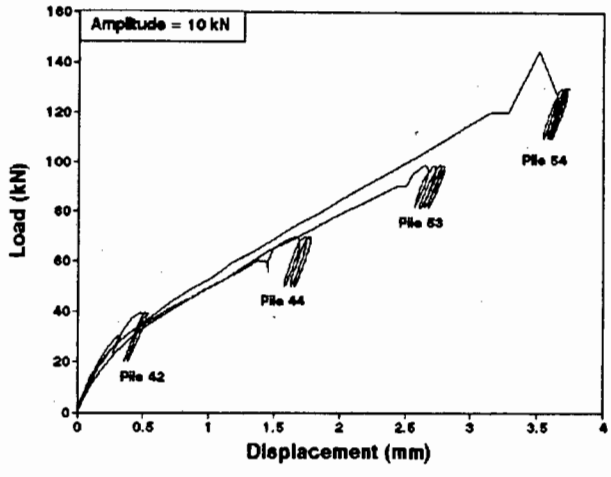

Figure 7.5 : Load - displacement relationship of piles with amplitude of 10kN

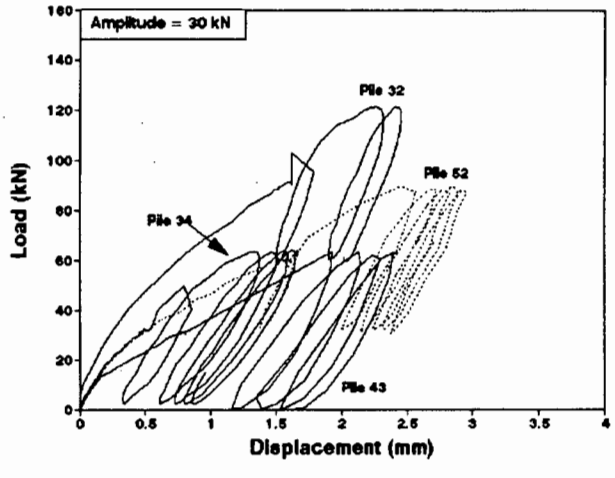

Figure 7.6 : Load - displacement relationship of piles with amplitude of 30kN

7.2.2 Displacement versus number of load cycles

The most common representation of cyclically loaded pile tests is in the form of the overall displacement of the pile head versus the number of applied load cycles. A typical example is presented in Figure 7.7 for the second cyclic load sequence of pile 42. Both curves, denoting upper and lower limits of the cyclic displacement, are almost parallel to each other. The vertical distance between the curves varies due to the hysteretic degradation which will be discussed in section 7.2.4. A zero displacement was assigned to the overall displacement at the start of the first cyclic sequence (upper limit of the first load cycle), thus ignoring the displacements during static loading.

This enabled a direct comparison of the cyclic behaviour of piles at different MCLVs which is shown in Figures 7.8 to 7.10. The displacements indicated are the maximum recorded during the respective load cycles. Each curve shows, therefore only the upper limit of load and displacement during cyclic loading.

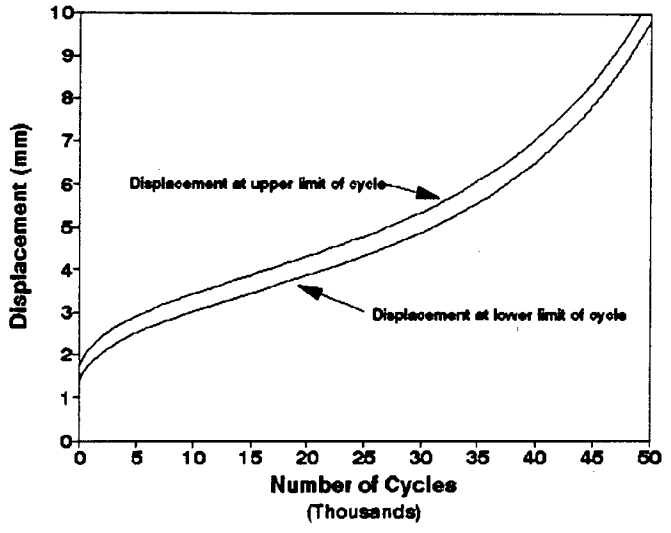

Figure 7.7 : Displacement envelope during the 2nd cyclic sequence of pile 42

a) Consideration of amplitude

In order to demonstrate the effect of the load amplitude on the pile displacement during cyclic loading, the pile responses are compared at fixed MCLVs of 30, 60 and 90kN in Figures 7.8, 7.9 and 7.10, respectively. Amplitudes range between 10kN and 30kN. Pile 42 (Figure 7.8), at an amplitude of 10kN (5% of ultimate load), shows negligible displacements during the period of cyclic loading. Piles 34 and 43, both with larger amplitudes of 30kN (15% of ultimate load), undergo a rapid increase in displacement with increasing number of cycles.

The appropriate piles with a MCLV of 60kN are presented in Figure 7.9. Pile 44, with a low amplitude of 10kN, shows an initial rapid increase in displacement which slowly decreases until no further significant penetration into the sand bedding occurs until completion of the test after 108 000 cycles of loading. Pile 51, with an amplitude of 20kN (10% of ultimate load), shows a similar trend, however, the slope of the curve (rate of penetration) is greater. A gradual increase in the slope is

recorded after about 80 000 cycles. Pile 52, with an amplitude of 30kN (15% of ultimate load), shows a remarkably different trend. The displacement increases far more rapidly than for the lower amplitude piles. It is worth mentioning that the displacements experience a distinct characteristic behaviour of exactly the same shape as the other two piles. However, this action (not visible in the scale of the figure) all occurs within a short period of cyclic loading. Until about 4 000 cycles the slope of the curve decreases after which it rapidly begins to increase.

Finally, piles with a MCLV of 90kN are compared in Figure 7.10. The trends for the low and high amplitudes are the same as those observed in the pile tests with MCLV of 30kN and 60KN (Figures 7.8 and 7.9). The curve of pile 32 (30kN amplitude) shows an initial decrease in slope, followed by a rapid increase after about 8 000 cycles. Pile 53 (10kN amplitude) on the other hand shows little penetration into the sand.

It is evident from the above results that the amplitude has a great effect on the pile behaviour for all MCLVs. The higher the amplitude the more rapid the increase in displacement.

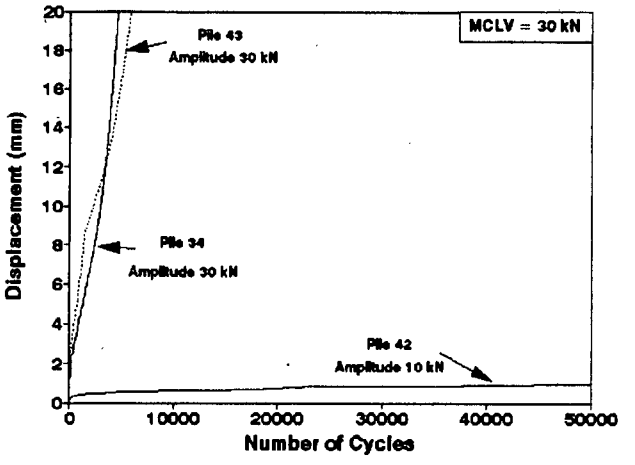

Figure 7.8 : Displacement - number of cycles relationship of piles with MCLV of 30kN

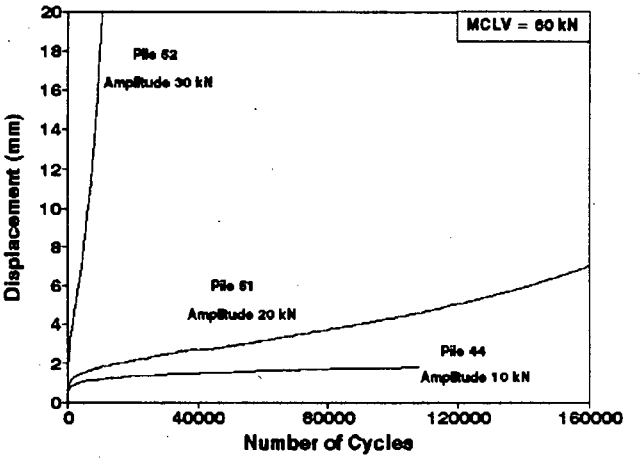

Figure 7.9 : Displacement - number of cycles relationship of piles with MCLV of 60kN

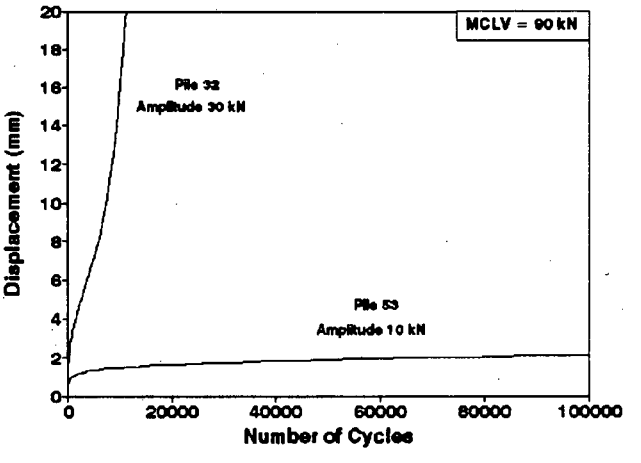

Figure 7.10 : Displacement - number of cycles relationship of piles with MCLV of 90kN

b) Consideration of MCLV

The displacements of the piles as a function of the MCLV during cyclic loading are shown in Figures 7.11 and 7.12. Responses of the piles subjected to amplitudes of 10kN and 30kN are presented.

The curves for piles with an amplitude of 10kN are shown in Figure 7.11. The overall shapes of the curves for the MCLVs of 30, 60 and 90kN are very similar. Generally, the piles undergo a rapid increase in displacement during the initial few thousand cycles after which the increase in displacement reduces to an almost constant value. A pile with a higher MCLV produces an increased displacement during the initial few thousand cycles. Thereafter the curves show almost identical trends. Again, pile 54 disturbs the regular pattern due to its average diameter being greater than the other piles. Temporary electronic noise due to a malfunction in the controller resulted in slight changes of the MCLV and therefore of the displacement response too. It is of interest to note that after the initial 5 000 cycles, these piles exhibit an increase in displacement of less than 1mm during the following 103 000 cycles. This suggests that the MCLVs investigated in this work have very little effect on the pile behaviour for amplitudes of 10kN.

This is in direct contrast to the displacement - number of cycles relationship which the piles subjected to an amplitude of 30kN show in Figure 7.12. The curves show a rapid increase in the displacement with increasing number of cycles. Piles 52 (MCLV 60kN) and 32 (MCLV 90kN) have identical responses up until 2 500 cycles after which the displacement of pile 52 increases more rapidly than that of pile 32. Pile 34, with the lowest MCLV of 30kN, produces the greatest increase in displacement with number of cycles. All the piles show an increase in the slope of the displacement-number of cycles curve after an initial transition phase of decreasing rates of displacements.

The above relationships indicate that if piles are subjected to an amplitude of 30kN, an increase in the MCLV causes a reduction of the displacement at a specific number

of cycles - as opposed to the 10kN amplitude piles in Figure 7.11. An increase in MCLV therefore appears to have a more positive effect on the pile performance for piles with amplitudes of 30kN. It should, however, be noted that for these MCLV/amplitude combinations the displacements are excessive after relatively few load cycles.

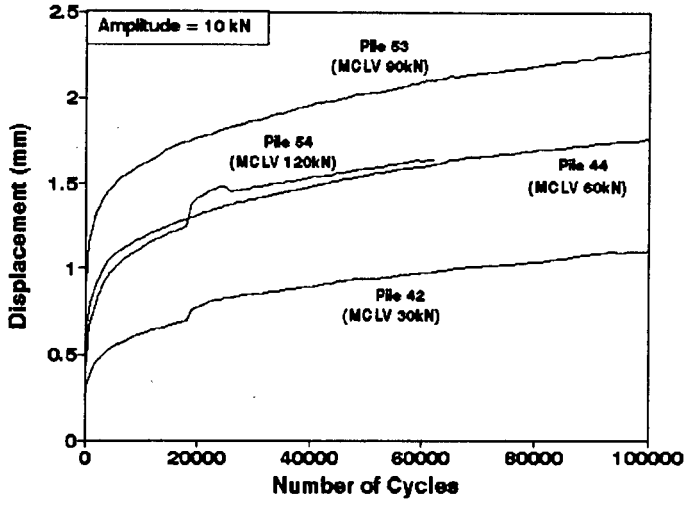

Figure 7.11 : Displacement - number of cycles relationship of piles with amplitude of 10kN

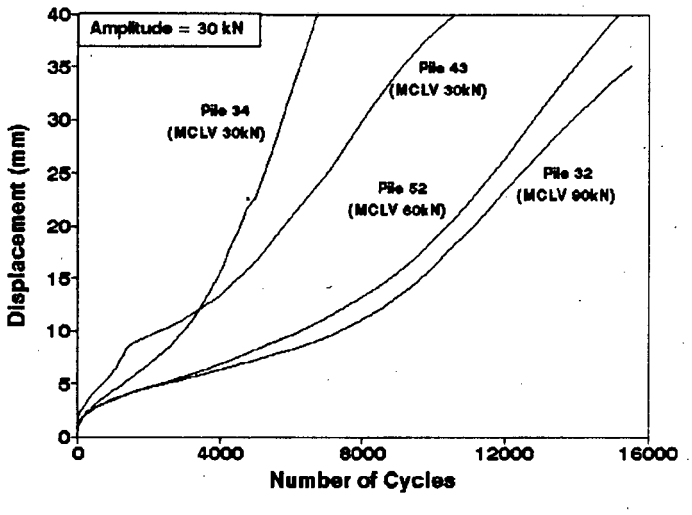

Figure 7.12 : Displacement - number of cycles relationship of piles with amplitude of 30kN

7.2.3 Rate of displacement versus number of load cycles

The gradient of a curve in the displacement versus number of cycles diagram represents the rate of displacement of a pile. The rate of displacement per load cycle was calculated by taking the change in displacement over an interval of either 500 or 1 000 cycles and dividing this displacement by the number of cycles in that interval. The interval size depended on the rate of movement of the pile. The smaller interval was selected during periods of high displacement rates. Checks using smaller intervals proved the consistency of the chosen method of rate evaluation. Again, the displacements considered were those at the peak of the load cycles.

In Figures 7.13 to 7.17 the rate of displacement versus number of cycles relationships for the piles tested are shown. In the figures on the left hand side of the page (denoted by 'a') these relationships are plotted using linear scales while in the figures on the right hand side (denoted by 'b') the scales of representation are logarithmic.

The general trend in all figures indicates that initially a relatively high rate of displacement is observed as cyclic loading begins. The rate of penetration drops off fairly constantly which may continue throughout the test period if the pile is subjected to the appropriate MCLV/amplitude combination. Some piles, however, maintain a constant rate for only a short period of time (number of cycles), after which the rate increases again. The actual rate of increase depends on the amplitude and MCLV of the load.

a) Consideration of amplitude

The influence of the cyclic load amplitude, at various MCLVs, on the rate of displacement response of the piles is shown in Figures 7.13 to 7.15.

The rates of displacement during the first 6 000 cycles for piles at a MCLV of 30kN are shown in Figure 7.13a with linear scales. The rate of pile 42, at a low amplitude of 10kN, decreases from an initial high value to a lower, almost constant, rate of

about $5*10^{-6}$ mm/cycle. This rate is maintained for the rest of the test up to 108 000 cycles (not shown in figure). Pile 34, at an amplitude of 30kN, shows a decrease in rate to a minimum value of about $2.4*10^{-3}$ mm/cycle. This rate is maintained for about 800 cycles following which it increases. In order to quantify the differences in rate it is of interest to note that the minimum rate observed from pile 34 is about 500 times larger than the minimum rate of pile 42 at the lower amplitude.

A more convenient and informative method of displaying this data is in terms of the logarithm of both the rate of displacement and the number of cycles as shown in Figure 7.13b. It is a widely used method of presenting creep data of clays (Mitchell et al., 1968) and rates of displacement of repeatedly loaded anchors (Hanna et al., 1978). All the curves are linear in the initial ranges of cyclic loading. Pile 42 (10kN amplitude) maintains a constant slope while piles 34 and 43 (30kN amplitudes) show an upturn or increase in the rate of displacement indicating rapid penetration of the pile in the sand. The rate reaches a peak value after which, in the case of pile 43, a decrease in the rate of displacement is observed.

The rates of displacement for piles at a MCLV of 60kN are presented in Figures 7.14a and 7.14b. The curves for the 10kN and 20kN amplitudes are very similar for the initial 40 000 cycles (not shown in Figure 7.14a). They indicate a decrease in the rate to low, almost constant, values of about $0.5*10^{-5}$ mm/cycle and $2.5*10^{-5}$ mm/cycle, respectively. Pile 44 (10kN amplitude) maintains this rate until the end of the test at 108 000 cycles while the rate of pile 51 (20kN amplitude) gradually increases after about 50 000 cycles. The rate of displacement of the 30kN amplitude pile (pile 52), however, decreases to a minimum value of $1.0*10^{-3}$ mm/cycle for about 850 cycles and then increases to a peak rate of $4.5*10^{-3}$ mm/cycle. The rate finally decreases again in the final stages of the test.

The trends observed in the logarithm plots of Figure 7.14b illustrate that the piles subjected to a larger amplitude reached the stage of increasing rate of displacement in a fewer number of cycles. The low amplitude pile (10kN) indicates no tendency for the rate to increase after the application of 108 000 load cycles.

The rate of displacement versus number of cycles relationship for the piles at a MCLV of 90kN are plotted in Figure 7.15a. The trends are similar for the piles at other MCLVs. The 10kN amplitude pile (pile 53) displays an almost constant rate of $5*10^{-6}$ while the 30kN amplitude pile (pile 32) maintains its constant rate of $8.4*10^{-4}$ mm/cycle for about 1600 cycles after which it increases to a peak rate of $3.9*10^{-3}$ mm/cycle. A decrease in the rate is observed after about 12 000 cycles. The log/log relationship of Figure 7.15b emphasizes these trends. Again, there appears to be a linear relationship between the displacement rate and the number of load cycles (in logarithmic scale) for piles subjected to an amplitude of 10kN.

The above results illustrate the effect of the amplitude on the rate of displacement of the pile head with increasing number of cycles. Generally, at all MCLVs an increase in the amplitude causes an increase in the rate of displacement after a fewer number of cycles and a larger minimum rate of displacement throughout these cyclic tests. A low amplitude of 10kN appears to have no effect on the rate of displacement at the MCLVs and the periods of loading experienced.

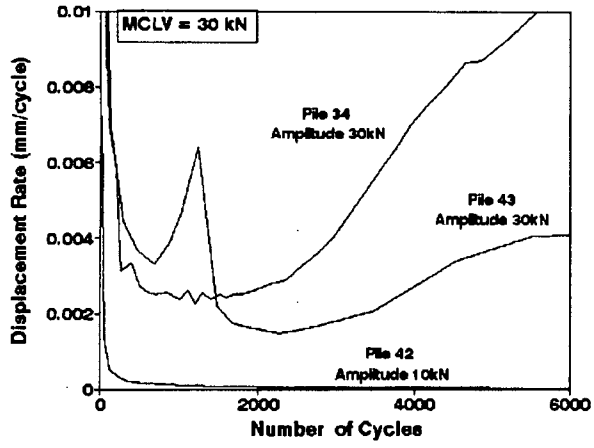

Figure 7.13a

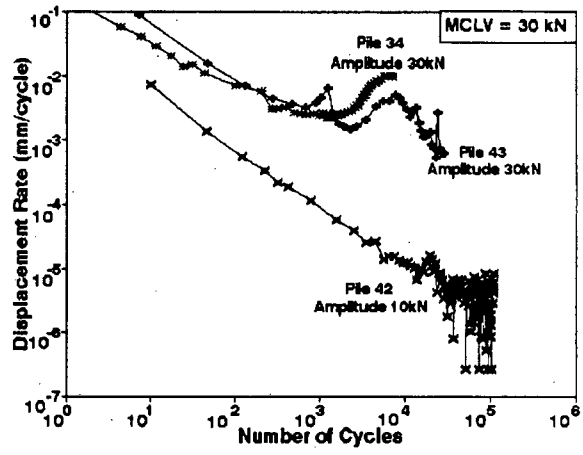

Figure 7.13b

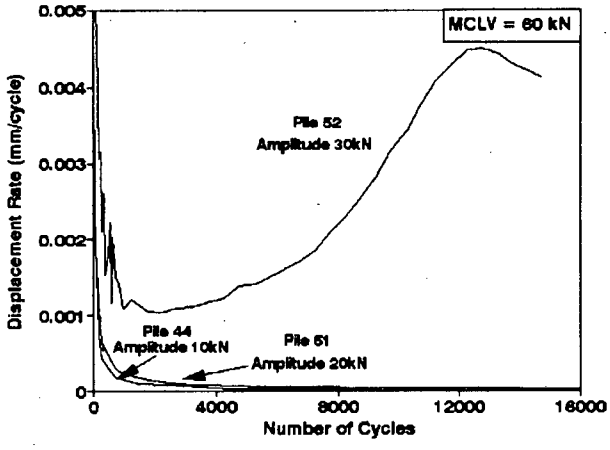

Figure 7.14a

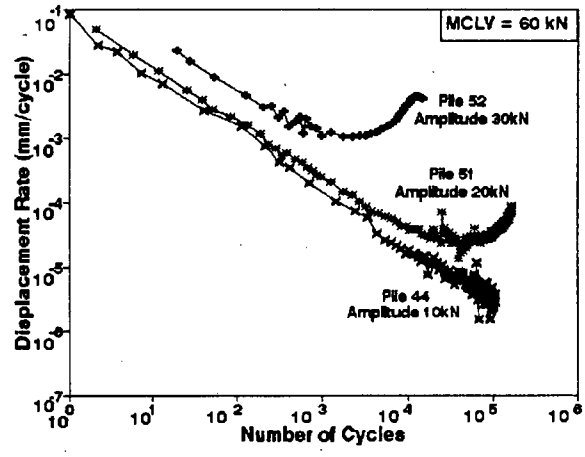

Figure 7.14b

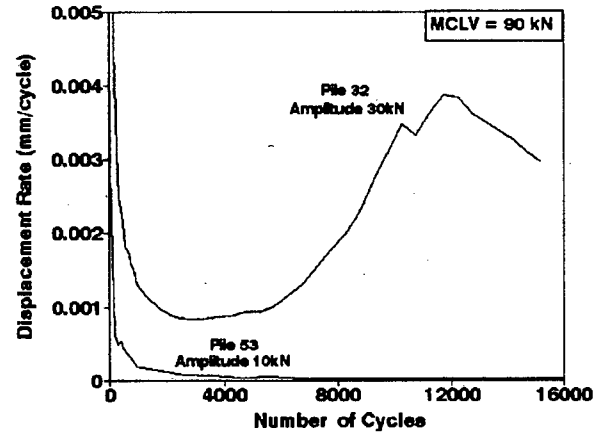

Figure 7.15a

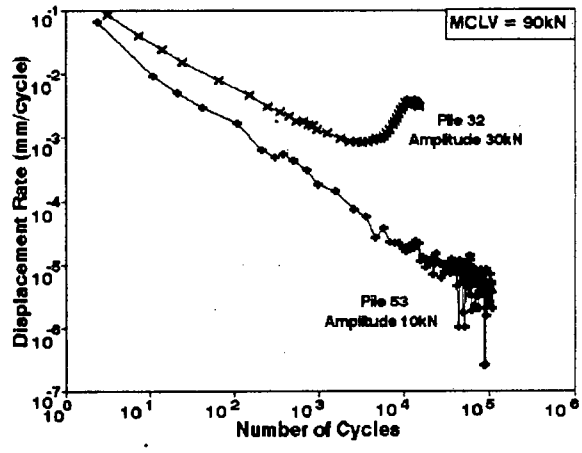

Figure 7.15b

Figures 7.13a,7.14a & 7.15a : Displacement rate - number of cycles relationship of piles with MCLVs of 30,60 and 90kN, respectively

Figures 7.13b,7.14b & 7.15b : Displacement rate - number of cycles relationship of piles with MCLVs of 30,60 and 90kN, respectively (logarithmic scale)

b) Consideration of MCLV

In Figures 7.16a and 7.16b the rates of displacement of piles, with varying MCLVs and constant amplitudes of 10kN, are depicted. From Figure 7.16a it can be seen that all the piles show an initial high rate of displacement which drops to about a constant value of $5*10^{-6}$ mm/cycle after about 30 000 load cycles. This rate is maintained throughout the test period of 108 000 cycles (graph is limited to 40 000 cycles).

During the initial 'settling-in' phase (up to about 10 000 cycles) it can be seen that, at a specific number of cycles, a lower MCLV produces a lower rate of displacement. Pile 54 disturbs the pattern due to its larger diameter as discussed previously. Beyond this phase the MCLV has very little influence on the pile behaviour.

In Figure 7.16b this trend is confirmed which supports the observations discussed earlier. In log/log representation these curves are straight lines, all showing the same negative slope, with some scatter at the ends. There is no indication of the piles deviating from this pattern.

The piles subjected to amplitudes of 30kN, however, react very differently at the various MCLVs. It is evident from Figures 7.17a and 7.17b that the piles at low MCLVs displayed higher rates of displacement than those at high MCLVs. At a given number of cycles these rates decrease with increase of MCLV. The pile with the minimum rate of displacement ($8.4*10^{-4}$ mm/cycle) has a MCLV of 90kN.

It is interesting to note that pile 34 tested at a relatively low MCLV of 30kN produces the greatest rate of displacement at any cycle number. The trend is significantly different to that of the piles tested at MCLVs of 60kN and 90kN. The rates of displacement of all the piles at amplitudes of 30kN decrease again after the peak rate is reached.

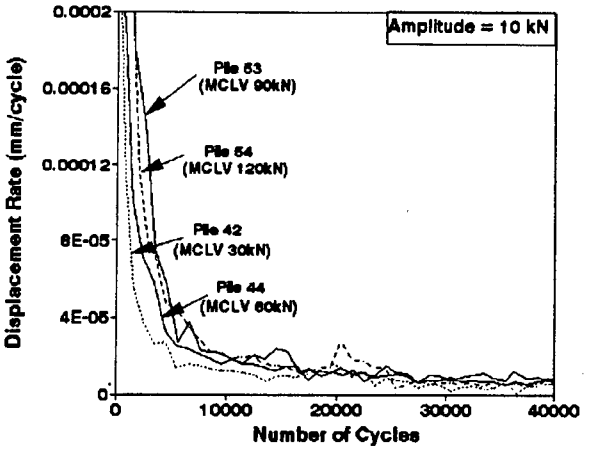

Figure 7.16a

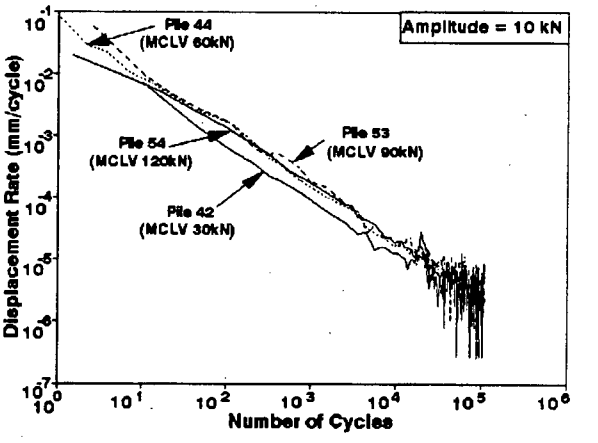

Figure 7.16b

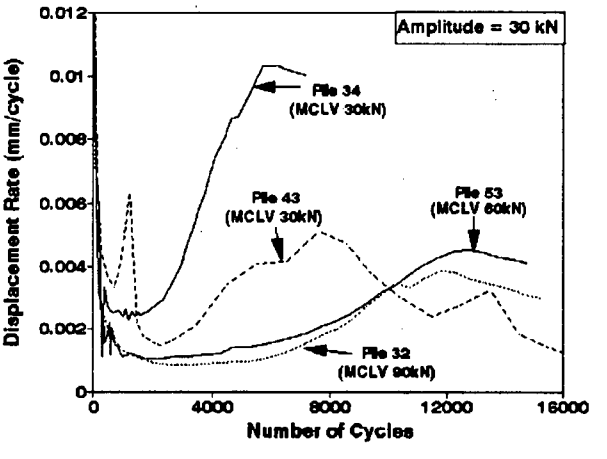

Figure 7.17a

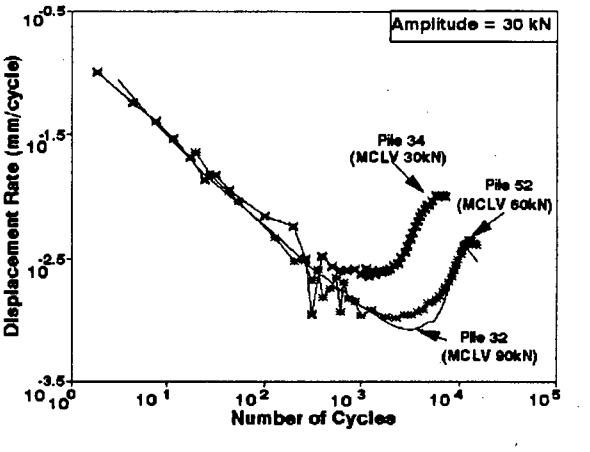

Figure 7.17b

Figures 7.16a & 7.17a : Displacement rate - number of cycles relationship of piles with amplitudes of 10kN and 30kN, respectively

Figures 7.16b & 7.17b : Displacement rate - number of cycles relationship of piles with amplitudes of 10kN and 30kN, respectively (logarithmic scale)

7.2.4 Cyclic load-displacement response

The continuous readings of the load-displacement response (during a particular load cycle) which are plotted in a load-displacement diagram, show a more or less closed flattened circle, termed a hysteresis loop. The shape and inclination of the loop gives an indication of the stiffness of the soil-pile system in terms of its elastic and inelastic components. The hysteretic response of the pile head recorded during cyclic loading is a function of the soil-pile interface response as well as the compressibility of the pile. The stiffness is the combined response of these two effects. Degradation in the soil-pile system stiffness is indicated in a decrease in the slope of the hysteresis loop.

In order to facilitate a quick and still fairly comprehensive analysis of the hysteretic behaviour of all the piles during the cyclic sequences, a linear regression line was fitted to the subsequent hysteresis loops at various intervals using the regression option of the computer package, Quattro Pro. The slope of the regression line represents a form of a soil-pile system stiffness modulus in analogy to the shear modulus derived from a stress-strain hysteresis loop in soil dynamics (eg. Hardin and Drnevich, 1972; Prakash, 1981). In Figure 7.18 one such hysteresis loop, with the fitted regression line, is shown. As discussed in section 5.3, the frequency of data acquisition was limited and hence the extra amount of data to be captured in the case of an instrumented pile meant that less load-displacement data was collected during one cycle in comparison to a non-instrumented pile. Therefore the hysteresis loops of the non-instrumented piles are more comprehensively defined.

In Figure 7.19 the results of these evaluations are shown in terms of the fitted stiffness modulus versus number of load cycles. Piles 31, 32 and 34 are not included due to the problems associated with the LVDT measurements during series 3.

The 10kN amplitude piles (denoted as A10) experience no significant degradation in the stiffness modulus. The piles, however, go through alternating periods of increasing and decreasing modulus, the average modulus being more or less constant. An increase in the MCLV has the effect of increasing the average stiffness modulus

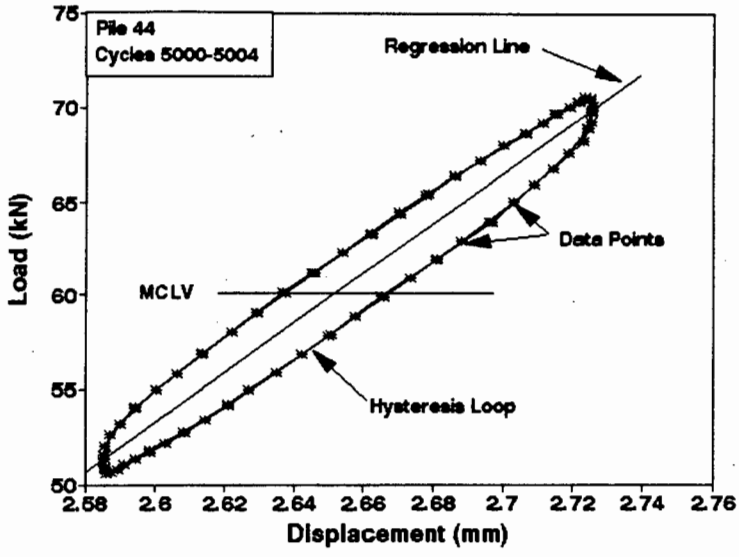

Figure 7.18 : Example of hysteresis loop with fitted regression line

of the pile but does not effect the degradation of the modulus. Pile 53 does not fit entirely into this pattern since the average stiffness modulus is lower than the other 10kN amplitude piles.

The piles with amplitudes greater than 10kN show a constant decrease in the stiffness modulus with little or no fluctuations. The rate of decrease in the stiffness modulus (slope of curve) increases with increasing amplitude.

Considering constant amplitudes (ie. 10kN or 30kN), the stiffness modulus at a specific number of cycles increases with an increase of the MCLV.

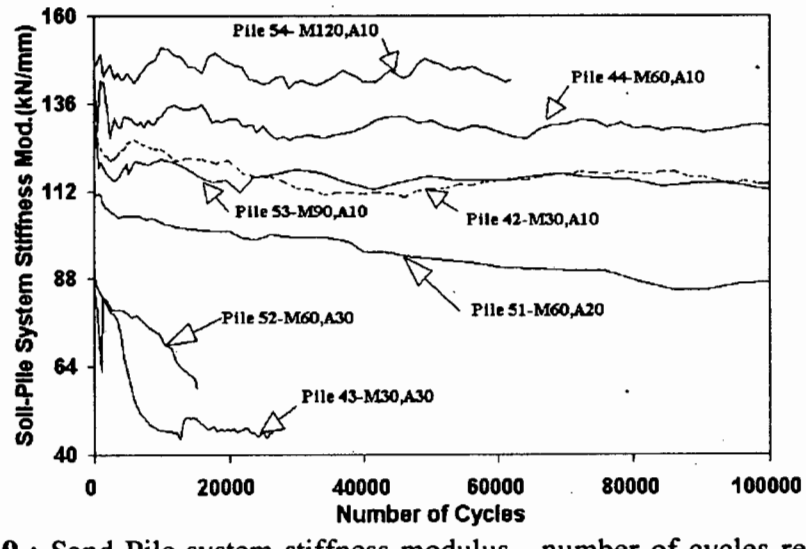

Figure 7.19 : Sand-Pile system stiffness modulus - number of cycles relationship

7.2.5 Ultimate load capacity after cyclic loading

After cyclic loading was completed the piles were unloaded and immediately statically reloaded to determine their remaining ultimate load capacity. In Figure 7.20 the load-displacement curves of the piles are shown. Again, the displacement at the start of reloading was assigned to zero for the purposes of comparison. One should bear in mind that the actual displacements involved are very different for the individual piles. The total number of load cycles completed also varies from pile to pile. Although it is difficult to compare these load-displacement curves, it is remarkable to note that the piles with the highest ultimate loads of about 186kN are those which were subjected to the smallest amplitudes during cyclic load application. Their load-displacement curves are significantly different to those of the curves of the 30kN amplitude piles which show ultimate loads ranging from 146kN to 166kN. Pile 42 seems to be an exception. A possible explanation could be the fact that, after the initial 108 000 cycles at an amplitude of 10kN, the amplitude was increased to 20kN for a further 290 000 load cycles. This pile has, therefore, been subjected to the greatest number of cycles (389 000) whilst having a more destructive amplitude during the latter sequence. This combined effect proved to be significantly more detrimental with respect to the ultimate load. When examining the 30kN amplitude piles it appears that the remaining ultimate load will be lower for piles subjected to longer periods of cyclic loading.

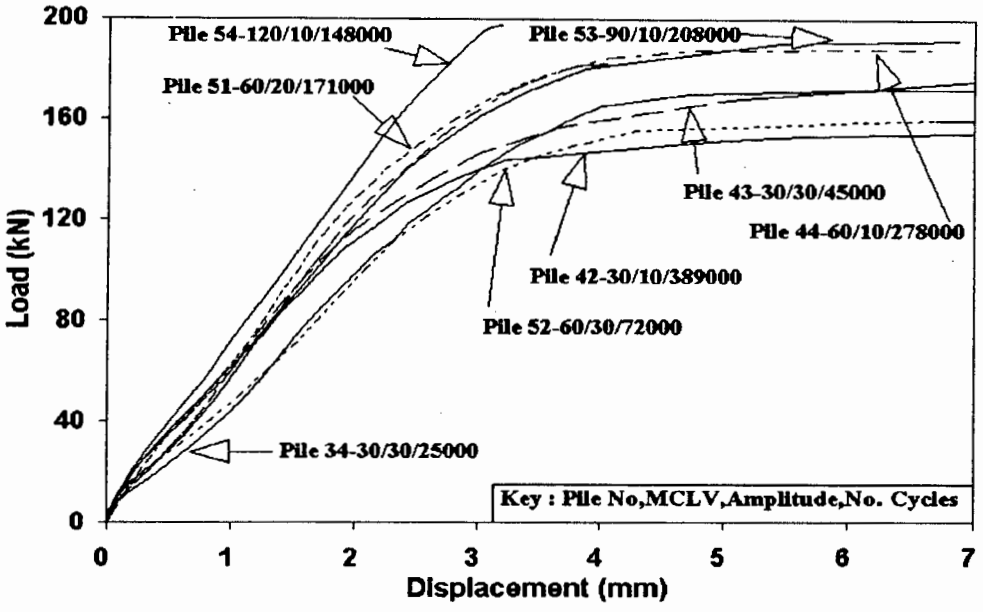

Figure 7.20 : Load - displacement relationship during determination of ultimate load capacity after cyclic loading

7.3 Internal Characteristics of Pile Behaviour

Five instrumented piles enabled a comprehensive analysis of the load transfer characteristics along the pile shaft to be undertaken. The information will definitely contribute to the interpretation and therefore understanding of the external characteristics of the pile behaviour.

7.3.1 Load distribution along pile shaft

The load at the gauge positions was calculated based on the assumption that the strain in the reinforcing bar, due to loading, was identical to the strain in the pile grout. This was considered reasonable as general engineering analysis of reinforced concrete assumes no bond slip (SABS 0100:1, 1992). Lee and Poulos (1991) also make the same assumptions in their work, although it is well established (Cornelius and Mehlhorn, 1982) that the strain in the reinforcing bar is not necessarily equal to the strain at the soil-grout interface at the same cross section. However, detailed research into this phenomenon was beyond the scope of this work.

In order to calculate the total load from the strain in the bar, the exact cross-sectional areas of the reinforcing and pile grout had to be determined. The area of the reinforcing bar was calculated as described in section 5.2.2. The pile cross-sectional area at the measuring points was calculated using the measurements of the external diameter of the piles at the respective cross sections after excavation. The actual grout area was then determined by subtracting the areas of the strain gauge covering and the cabling in the cross-sectional plane from the pile area.

The total load at the measurement point was calculated as follows:

$$Load = \epsilon \ (E_{steel} \cdot A_{steel} + E_{grout} \cdot A_{grout})$$

where : E = Young's modulus

ϵ = strain

A = cross-sectional area

Although the Young's modulus (E) of the grout was determined, there exists some doubt as to whether the value obtained is representative of the actual pile grout in general. Additionally, the grout quality may change along the pile shaft due to slight variations in the grout pressure during installation. Also the curing conditions along the pile shaft improve from top to bottom as the moisture content of the surrounding soil mass increases. These factors could result in higher E values near the pile tip. Another factor which could not be quantified was the possibility that during cyclic loading the actual modulus of the pile grout may have degraded. However, since these factors are not quantifiable a constant value of E was assumed along the pile shaft.

Errors that could not be eliminated were caused by the misalignment of the force and pile axis and possible curvatures in the actual pile shaft. Moments which developed out of the plane of the two gauges could also have caused erroneous strain readings. It was noticed that during attachment of the pile cap to the loading plate of the actuator, any moments introduced caused slight shifts in the strain readings.

Therefore, the strain gauges were monitored while the cap was tightened and any moments were eliminated by adjusting the bolts.

The distribution of load, at selected load levels, along the shafts of the instrumented piles is shown in Figure 7.21. The load in the piles decreases almost linearly with increasing depth. The magnitude of load at each gauge position increases with a corresponding increase in the applied load. The load distribution below the lowest measuring point is unknown and therefore the exact load at the tip of the piles is unclear. The presented load distributions concur with the observations of other researchers published in the respective research papers (Cooke et al., 1979; Lee and Poulos, 1991; Reese et al, 1969; Vesic, 1970).

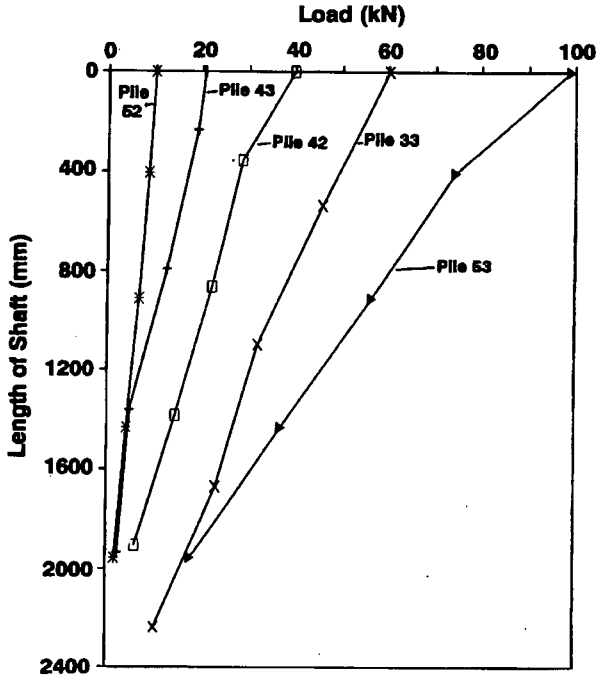

Figure 7.21 : Load distribution along pile shafts at selected loads

7.3.2 Skin friction distribution along pile shaft

The load transferred to the soil along the soil-pile interface is generally expressed in terms of skin friction. The major objective of this research was to investigate the skin friction characteristics along the pile shafts during cyclic loading in order to understand the interactions that take place along the interface.

a) Method of calculation

The skin friction distribution was determined by dividing the differences in load at adjacent measurement points by the respective average shaft area. The skin friction above the top gauges was calculated from the difference between the applied load and the load at those gauges. The skin friction below the lowest strain gauges was assumed to be the same as that just above them. At times an abnormally high load transfer (skin friction) was calculated in the upper section of the pile. This phenomenon was also discovered by Appolonia and Romualdi (1963) and Reese et al.(1969). It is believed that this is due to an eccentric load application thus causing a moment in the top section of the pile. Possible explanations could be slightly skew loading surfaces (pile cap surfaces) or some rotation of the pile itself.

In certain piles the initial strain gauge readings prior to the commencement of the test were quite different to those obtained during calibration of the reinforcing bar. This resulted in minor initial non-zero skin friction distributions along the pile shaft. There are a number of reasons for these residual values. Firstly, after casting, the pile grout undergoes shrinkage and temperature changes. These volumetric strains can cause relative displacements of points on the pile which may result in load transfer as stated by Touma and Reese (1974). Secondly, the self-weight of the pile and the settling of the sand after installation can cause some load transfer. It is, however, difficult to evaluate the effects of these strains and therefore the zero readings of the gauges at the start of the tests were used, thereby disregarding any initial strain conditions.

The skin friction distributions for all piles were analyzed at the upper and lower limits of a load cycle. Both distributions indicated the same trends, the only differences being the magnitudes of the skin friction. Therefore only the results of the peak points (ie maximum skin frictions) are presented.

In order to illustrate the redistributions and continuous changes of skin friction along the pile shaft during the application of cyclic load, a few distributions at selected numbers of cycles will be discussed.

b) Skin friction distributions due to low amplitudes at various MCLVs

It has already been mentioned that cyclic loading with an amplitude of 10kN had little effect on the load-displacement behaviour of a pile at the various MCLVs experienced. In Figures 7.22 and 7.23 the skin friction distributions of piles 42 and 53, after the indicated number of load cycles, are shown.

Along pile 42, at a MCLV of 30kN, a distinct redistribution of skin friction was observed. The skin friction at the two extremes of the pile, near the top and tip, decreased with an increase in the number of cycles whilst the central portion of the pile experienced an increase. Thus, the skin friction along the shaft was essentially mobilised to a maximum value of about 155 kN/m^2 and the skin friction at the tip did not develop. This confirms the fact that the pile underwent little penetration since the side shear (skin friction) still offered ample resistance against the applied cyclic loading.

Pile 53, at a MCLV of 90kN, showed a slightly different behaviour in terms of the skin friction distribution to that of pile 42. The skin friction along the top 600mm of the pile decreased continuously with an increase in the number of cycles, whereas a continuous increase was observed along the lower part of the shaft. A significant difference to that of pile 42 is the fact that the skin friction at the pile tip was mobilised. It reached a 'peak' value of 165 kN/m^2 at which point it appears that some state of equilibrium was achieved and maintained throughout the entire test of 108 000 load cycles.

During the second load sequence for both these piles, at an amplitude of 20kN, it was observed that the "peak' skin friction increased substantially thereby establishing that

the skin friction had indeed not been fully mobilised during the low amplitude loading.

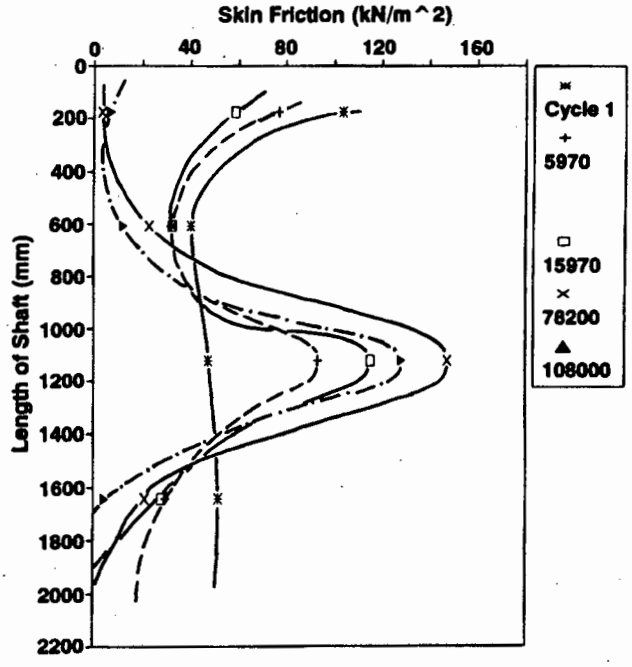

Figure 7.22 : Skin friction distribution along shaft of pile 42 (MCLV=30kN, Ampl.=10kN)

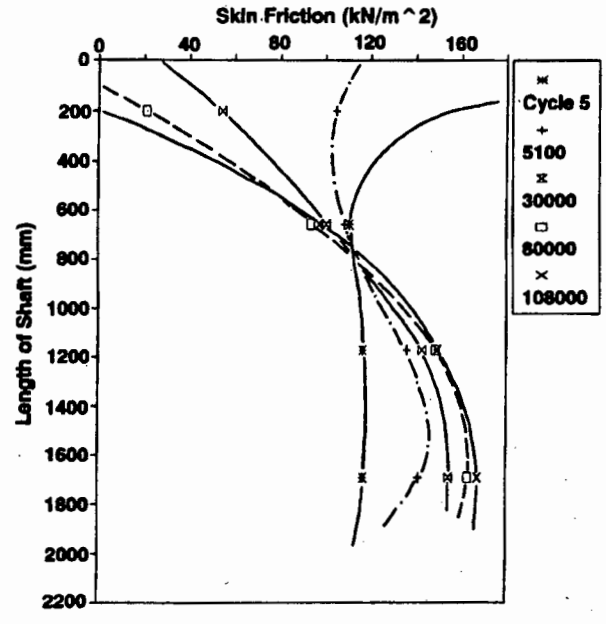

Figure 7.23 : Skin friction distribution along shaft of pile 53 (MCLV=90kN, Ampl.=10kN)

Comparison of these two piles shows that the higher MCLV of 90 kN, together with the associated greater displacement, led to the mobilisation of skin friction at the lower part of the pile near the tip and a consequent rapid decrease in skin friction at the top of the pile after a few load cycle applications.

c) Skin friction distribution due to high amplitudes at various MCLVs

The detrimental effect of the 30kN amplitudes at the tested MCLVs on the load-displacement behaviour of the piles was established earlier. The two piles (43 and 52) subjected to amplitudes of 30kN at MCLVs of 30kN and 60kN respectively, were selected as representative examples of piles subjected to this cyclic load combination (Figures 7.24 and 7.25). A marked difference in the skin friction distributions to those of piles 42 and 53, subjected to amplitudes of 10kN, is apparent. The top 600mm of both shafts again experienced a continuous decrease in skin friction with the increasing numbers of cycles. However, all positions along the lower part of the shafts showed an initial increase in skin friction to a maximum, followed by a decrease to a significantly lower value (Cowburn and Scheele, 1993). The decreases were associated with increases in skin friction at lower depths. It appears that the peak skin friction moved progressively towards the tip of the piles after which it decreased to a near constant residual distribution of about 30 kN/m^2. This is clearly evident for pile 43 after 7080 cycles. The skin friction near the tip of pile 43 showed a sudden increase after 7080 cycles while the residual shear stress remained constant at all other locations.

A very significant observation was the fact that at the moment the skin friction had reached the peak value at the pile tip and subsequently decreased, the rate of the displacement of the pile started to increase. This occurred after 1780 and 3500 load cycle applications of pile 43 and 52 respectively.

The same observation was made during the second sequence of loading (20kN amplitude) of the piles initially subjected to a 10kN amplitude (piles 42 and 53). Thus the conclusion can be drawn that the rate of displacement of a pile starts to increase

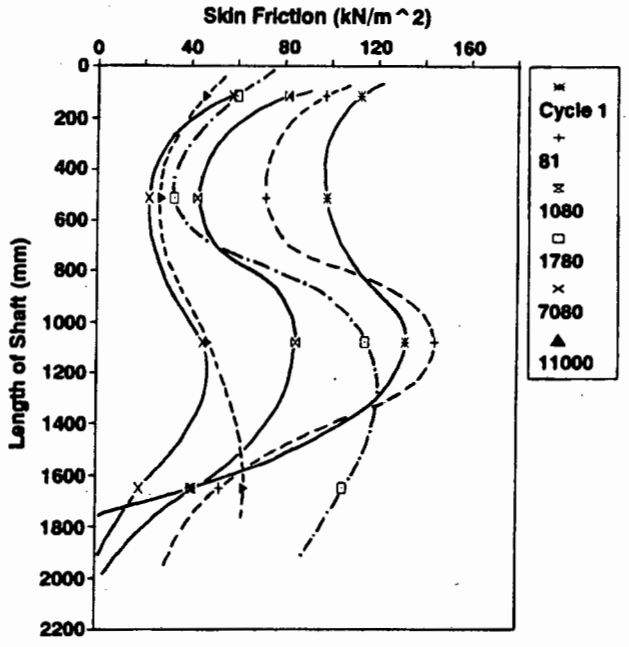

Figure 7.24 : Skin friction distribution along shaft of pile 43 (MCLV=30kN, Ampl.=30kN)

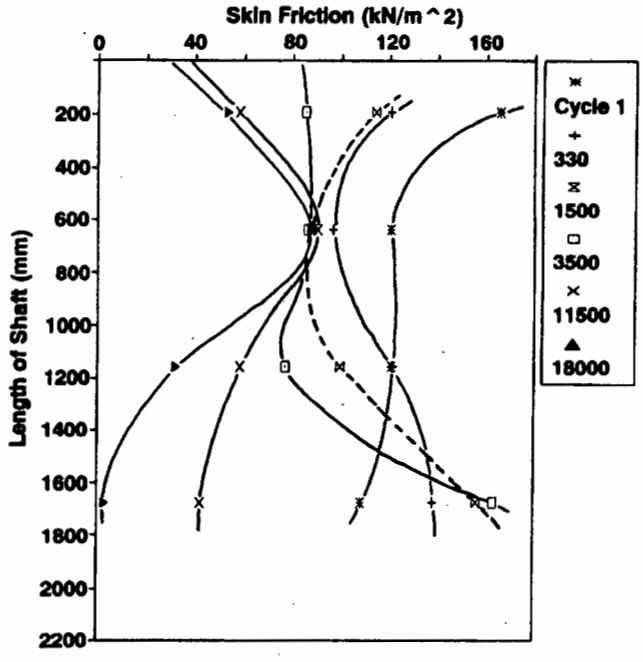

Figure 7.25 : Skin friction distribution along shaft of pile 52 (MCLV=60kN, Ampl.=30kN)

when the equilibrium between the applied load and side shear resistance (skin friction) is out of balance. Once the maximum skin friction at the tip of the pile has been overcome, the pile penetrates almost unrestricted into the subsoil since the skin friction along the shaft does not provide significant resistance. However, as soon as

the pile displaces the point resistance is activated. From this stage onwards the point resistance will provide the major resistance against continued loading.

There appears to be a relationship between the total displacement from the commencement of the test and the point at which the skin friction at the pile tip drops, and thus the rate of displacement increases. An analysis in this respect showed that all the piles were displaced by about 9.6mm when this occurred - this is about 9.5% of the pile diameter (ϕ). The total displacements at the respective number of load cycles, at which the skin friction at the pile tip drops, are listed in Table 7.4. All the piles for which this observation was made are included in the evaluation.

Table 7.4 : Displacement and number of cycles when point skin friction at pile tip drops

Pile No.	Displ. when skin friction drops or displ. rate increases. (mm)	Displ. as % of pile ϕ (%)	Cycle No.
32	10.0	9.9	5 500
34	9.0	9.0	2 300
41	11.0	10.9	13 000
43	10.8	11.1	1 780
44 (2nd Seq.)	10.5	10.3	72 000
51	7.5	7.2	140 000
52	9.0	9.0	4 000
53 (2nd Seq.)	9.4	9.3	32-49 000
54 (2nd Seq.)	9.2	9.0	85 000
Average	9.6	9.5	-
Std Dev.	1.1	1.19	-

The results show an average displacement of 9.6mm with a standard deviation of 1.1mm. Assuming a student-t distribution it is found that 95% of all possible sample means will fall within $\pm$ 0.91% ϕ of the population mean. The results therefore predict with 95% certainty the displacement range when the degradation of the skin friction at the pile tip starts and the rate of pile penetration increases. This is equivalent to a displacement of 8.6% to 10.4% of the pile diameter.

7.3.3 Point resistance of piles

The total resistance of a pile to loading is provided by a combination of the shear resistance (skin friction) and the point resistance. In the case of these research piles in the sand embedment, the resistance is principally derived from the shear resistance along the shaft in the initial stages of cyclic loading. The short, stiff piles have a low compressibility and hence the tip experiences a displacement at relatively small loads. This displacement in turn induces a bearing stress. The displacement required to achieve full load transfer along the shaft is very small whereas a large displacement is needed to develop full point resistance (Poulos, 1981b; Touma and Reese, 1974).

The load at the tip was estimated by calculating the total load transferred via shaft friction and subtracting it from the applied load. The total shaft load was estimated by multiplying the average skin friction between each measurement point by the average pile surface area between those points.

The point load development during the cyclic load tests is shown at the upper limits for two selected piles in Figures 7.26 (pile 53) and 7.27 (pile 52). The general shapes of the curves are similar to those of their respective displacement - number of cycles relationships (see Figures 7.11 and 7.12 in section 7.2.2). Considering pile 53 (MCLV=90kN, Ampl.=10kN), a relatively high initial point load (11% of applied load), due to a high MCLV, is calculated at the start of cyclic loading. The point load increases rapidly during the first few thousand cycles. It stabilises to a constant value of about 21% of the applied load or 21kN. This value corresponds to a point bearing stress of 2.86MPa at a total displacement of 4.9mm. In the stress calculation the actual pile tip area, which was measured after pile excavation, was taken into account. The point load shows intermediate fluctuations due to local rearrangements of the grain structure below the tip.

Pile 52, at a MCLV of 60kN and an amplitude of 30kN, shows four distinct stages in the development of the point load. Initially, the load increases rapidly after which a short period of a constant tip load of about 11% of the applied load is established.

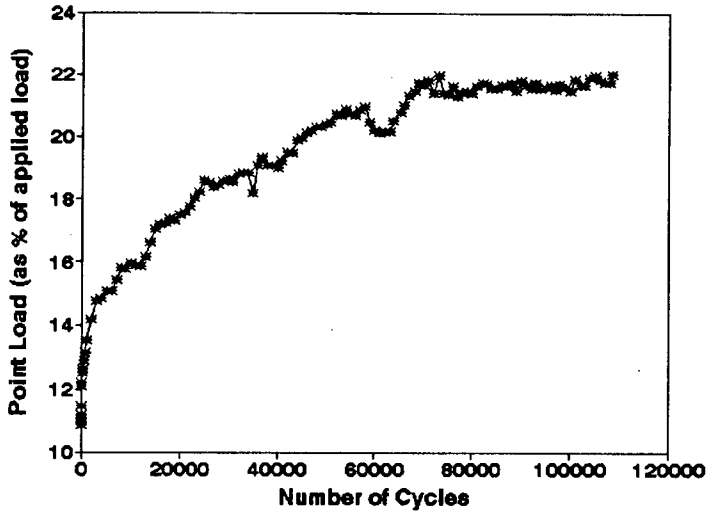

Figure 7.26 : Point load - number of cycles relationship of pile 53 (MCLV=90kN, Ampl.=10kN)

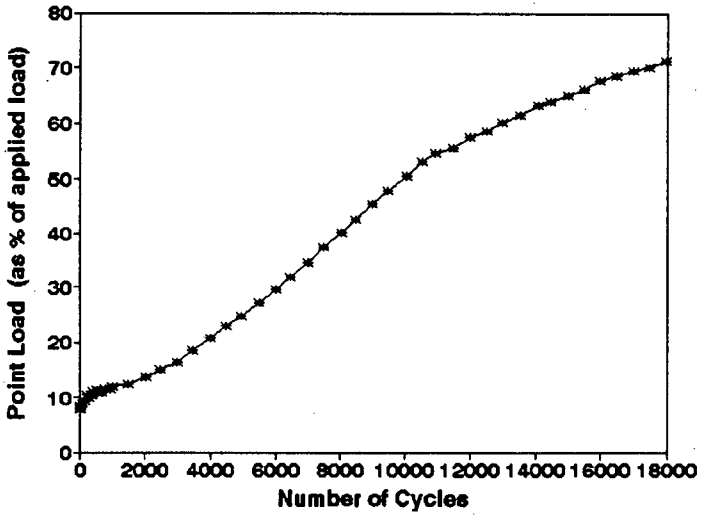

Figure 7.27 : Point load - number of cycles relationship of pile 52 (MCLV=60kN, Ampl.=30kN)

This stage coincides with the observation of a constant rate of displacement at the pile head. Thereafter the point load increases continuously, again corresponding to the degradation (decrease) of the skin friction along the shaft. After a period of about 104 000 load cycles a minor decrease in the slope of the curve is observed. The point load at the end of the test is 67% of the applied load or 60kN. This is equivalent to a point bearing stress of 8.4MPa. The total displacement at this stage is 42mm.

Static tests were previously undertaken (Schwaeble, 1991) in order to establish the maximum point bearing stresses to be expected in an equivalent sand bed (same soil

mechanical properties). The objective was the experimental determination of the ultimate load capacity of a circular steel plate of 90mm diameter at various depths within the sand mass. The results, shown in terms of contact pressure (point bearing stress) versus displacement in Figure 7.28, indicate that at embedment depths of 1m and 2m very little change in the ultimate capacities was observed. This supports the statement of Touma and Reese (1974) that below a certain critical depth the ultimate unit resistance of the pile tip resistance remains more or less constant for model piles in sand. The critical depth was identified as ranging from 10 times the pile diameter in loose sand to 20 times the diameter in dense sand embedments. This corresponds to depths of between 1m and 2m in the sand mass used in this research.

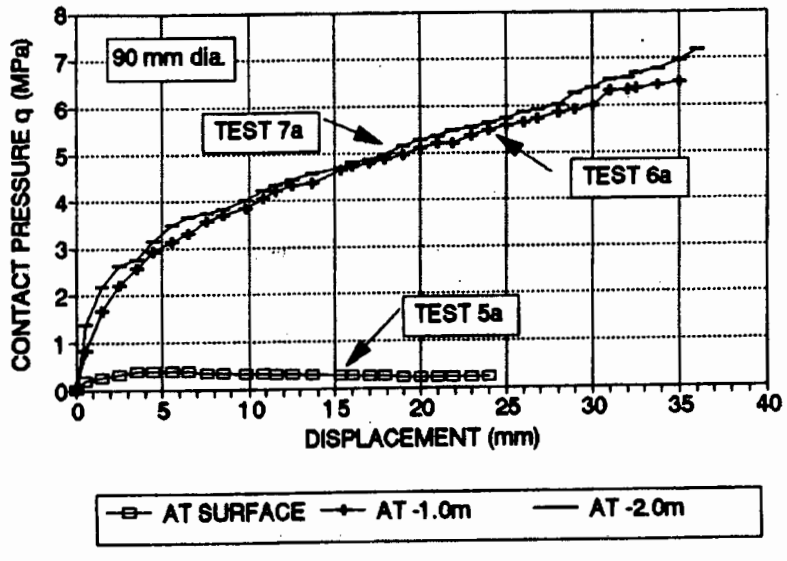

Figure 7.28 : Contact pressure - displacement relationship of steel plates at various depths within the sand mass (after Schwaeble, 1991)

The bearing capacity tests at 1m and 2m depths did not produce the classical failure (penetration without increase in load). However, a slow increase in contact pressure with an increasing displacement was observed. The point bearing stresses calculated for the piles 52 and 53 and the contact pressures below the plates at corresponding displacements are listed in Table 7.5.

Table 7.5 : Point bearing and contact stresses at selected displacements

Pile No.	Displacement of pile (mm)	Point bearing stress at pile tip (MPa)	Contact stress of plate (Schwaeble, 1991) (MPa)
52	42.0	8.4	7.8 (extrapolated)
53	4.9	2.9	3.3

The similarity of the point bearing and contact stresses at the same displacements is remarkable even though the diameters are not exactly the same.

To generalise, it can be stated that the point resistance increases with an increasing number of load cycles and it appears that the point load of the piles subjected to low amplitudes (10kN) rises to a maximum value which is maintained during the subsequent cyclic loading. The point resistance of piles subjected to high amplitudes (30kN), however, continually increases with the number of load cycles.

7.3.4 Analysis of hysteretic behaviour at pile tip

The hysteretic behaviour of the pile head is a function of the sand-pile response as well as the compression of the pile itself. The extent of the pile compression was therefore estimated using the strain measurements along the shafts of the instrumented piles. The strain was calculated from the bridge equations as explained in section 5.2.2.

The total compression of the piles was estimated at both the upper and lower limits of the load cycles as follows:

$$Total\ compression = \sum_{n=1}^{4} (\epsilon_n * l_n)$$

where n = measurement point number

ϵ_n = strain at measurement point n

l_n = length of shaft per measurement point n

In order to provide a check to determine if these calculated displacements (compressions) were correct, a theoretical method was used to calculate the pile compression. This method involved the calculation of the compression of the whole pile assuming it to be only end-bearing on a rigid foundation or, in terms of structural analysis, a reinforced column with a fixed end condition.

Considering the stiffening effects of the reinforcing on the pile shaft, an effective grout area was calculated (SABS 0100-1, 1992) as follows :

$$A_{eff} = A_{grout_{(gross)}} + (\alpha_e - 1) A_{steel}$$

where $A_{grout_{(gross)}}$ = gross area of grout (including steel)

A_{steel} = area steel

α_e = ratio of Young's moduli of steel to grout

From this relationship the stress and strain in the pile was determined from :

$$\sigma = \frac{Force}{Area_{grout}} \qquad hence \qquad \epsilon = \frac{\sigma}{E_{grout}}$$

where E_{grout} = Young's modulus of grout

The results of this investigation are listed in Table 7.6. The net change in the displacement of the pile head (ΔD_h) during one load cycle is determined from the linear potentiometer readings and is shown schematically in Figure 7.29. This is compared to the net change in the pile length (Δl) due to compression during that same load cycle. If the contribution from the compression (Δl) is then subtracted from the net pile head displacement change (ΔD_h), the change in the displacement of the sand below the pile tip (ΔD_s) during the specific load cycle is obtained. This represents the elastic response of the sand below the tip.

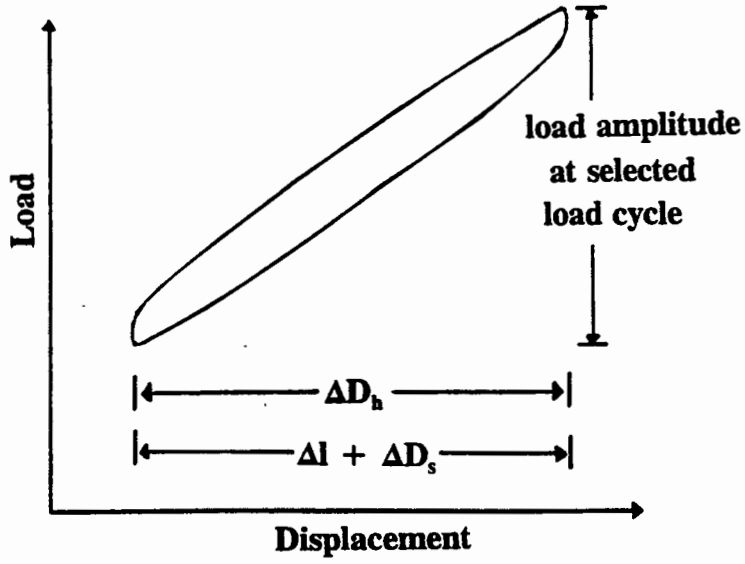

Figure 7.29 : Schematic of variables used in calculation of elastic compression of sand

Pile No.	MCLV/ Amplitude (kN)	Cycle Number	Observed Change in Displ. of Pile Head (ΔD_h) (mm) A	Observed Compression in Pile from Strain Gauges (Δl) (mm) B	Elastic Displ. of Sand Below Tip (ΔD_s) (mm) A-B	Calculated Change in Compression of Pile (assumed only end-bearing) (mm)
42	30/10	1 000	0.16	0.12	0.04	0.28
		100 000	0.17	0.12	0.05	0.28
53	90/10	10 000	0.15	0.13	0.02	0.36
		100 000	0.16	0.13	0.03	0.36
43	30/30	1 000	0.99	0.54	0.45	1.01
		10 000	1.30	0.63	0.67	1.01
52	60/30	800	0.67	0.49	0.18	1.07
		15 000	0.96	0.57	0.39	1.07

The change in displacement during a load cycle which was calculated assuming the pile to be end-bearing on a rigid foundation gives a larger value than that calculated from the actual strains along the pile shaft. This was expected due to the skin friction resistance acting along the shaft. The magnitudes of the response are greater for the 30kN amplitudes and all the piles show an increase in the elastic sand response with an increase in the number of cycles. Unfortunately, since there is only limited data available (ie. only 4 instrumented cyclic pile tests) no comparisons of the effects of the MCLV and amplitude on the sand response below the tip can be made. However, these results are a foundation for future research which has been initiated, namely the

the MCLV and amplitude on the sand response below the tip can be made. However, these results are a foundation for future research which has been initiated, namely the investigation of the micro-mechanical processes occurring in the contact zones of piles and sand.

CHAPTER 8:
SUMMARY AND INTERPRETATION OF RESULTS

The observations regarding the displacements of the pile heads during cyclic loading, the rates of displacement, the hysteretic behaviour during a load cycle, the ultimate loads after cyclic loading, the skin friction development along the pile shafts and subsequent establishment of the point resistance indicate that the effects of the amplitude and the MCLV must always be considered together. This was also highlighted by Poulos (1988) in his conclusions on cyclic stability.

The results are summarised in this chapter in the same order in which they were presented in chapter 7. An attempt is made to interpret the experienced trends.

Static Load-Displacement Response : The high degree of similarity between the initial static load-displacement curves of the piles demonstrates that the test methods applied and executed in these experiments; which consisted of sand preparation, pile installation and test loading; were of good reliability and accuracy. This was a prerequisite in order to facilitate direct comparisons of the pile responses under the different load conditions. The initial displacements of all the piles prior to the commencement of cyclic loading can be determined from these curves. These displacements should be considered when comparing the pile behaviours, particularly the skin friction development, as the displacement-number of cycles relationships presented assume zero displacements at the start of cyclic loading.

Displacement versus number of load cycles : The displacement-number of cycles behaviours for all the piles are shown in Figure 8.1 in a single graph to illustrate clearly the differences in pile behaviour due to variations in the cyclic load amplitudes only. It should be noted that in this presentation displacements at the start of cyclic loading were set to zero to allow for a comparative study.

The initial displacement development, ie. loading from zero load to the MCLV, must always be considered in all the following considerations. In order to simplistically emphasize this point, the skin friction development and a classical shear-displacement relationship of a medium dense sand material (Terzaghi and Peck, 1948) may be related. A large (initial) displacement, due to a high MCLV, activates a high shear stress at the sand-pile interface. Any minor increase in the shear stress (skin friction) due to a cyclic load, assuming some amplitude, may mobilise fully the shear potential of the sand and even overcome the peak values, thus initiating degradation with each subsequent load cycle. On the contrary, a low MCLV and small amplitude inflicts only small displacements which are associated with low shear stresses. This cyclic loading is likely to change these stresses only insignificantly and thus many more load cycles would be required to reach the stage of degradation. A high amplitude at this low MCLV may result in a range of shear stress from full development to almost complete 'relaxation' during a load cycle which causes the most severe degradation within the shear interface.

As shown in Figure 8.1 the piles with 10kN amplitudes show relatively little penetration into the sand during cyclic loading. This highly stable behaviour which prevails over many thousands of low amplitude load cycles confirms the observations of Chan and Hanna (1980). The pile with a greater amplitude of 20kN displays a similar behaviour to the piles with 10kN amplitudes during the initial stages of cyclic loading. However, the magnitude of displacement at any load cycle is greater. In contrast, the displacements of the piles with 30kN amplitudes increase rapidly with increasing load cycles and all displacements exceed 10mm in less than 10 000 cycles, while piles subjected to other amplitudes never achieved this displacement during the test period. The curves show a distinct grouping according to the load amplitude. Thus it can be concluded that the higher the amplitude of cyclically loaded piles the greater the displacement (penetration) for a given number of cycles.

The increase in the displacement with amplitude is proportionately smaller from 10kN to 20kN than for the increase from 20kN to 30kN. This suggests that there may be a critical amplitude above which the pile displacement increases very rapidly with an increase in the number of load applications. This result confirms the concept of a critical level as

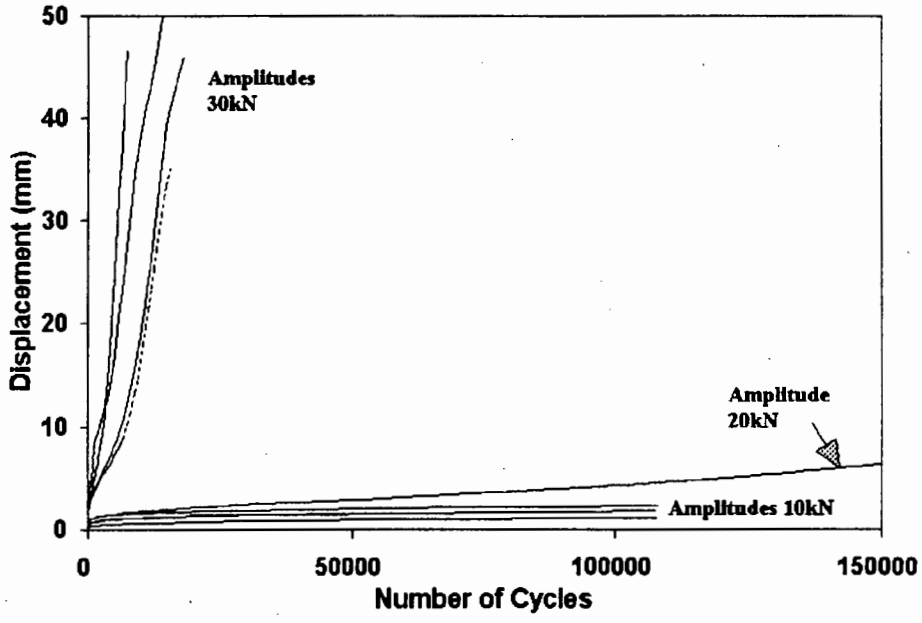

Figure 8.1 : Displacement - number of cycles relationship of all test piles stated by Chan and Hanna (1980), Poulos (1981b) and Lee and Poulos (1991).

The influence of the MCLV is not as obvious as that of the amplitude. At the lowest amplitude (10kN) an increase in the MCLV results in a certain displacement being achieved in a smaller number of load cycles. Conversely, at the highest amplitude (30kN) an increase in the MCLV produces a specific displacement after a larger number of cycles.

These trends can be interpreted as follows: in the low amplitude tests the magnitude of the stress reversals are relatively small and insignificant. This results in the amplitudes having little effect on the state of stress within the sand-pile system. However, the higher stress reversals associated with higher amplitudes are sufficient to affect negatively the equilibrium of the sand-pile system. In these cases the displacements become large after relatively few cycles and, together with a high MCLV, would cause high densities below the tip. The piles are least stable when the amplitude is equivalent to the magnitude of the MCLV as in the case of piles 34 and 43. This is in agreement with the observations of Hanna et al. (1978) that in anchors the most severe loading occurs when the system is completely unloaded during a cycle of loading. There is then a complete relaxation of stress at, and close to, the pile head.

Rate of Displacement of Pile Head : Similar trends, as established above, are observed when the rates of displacement of the pile heads with increasing numbers of cycles are compared. The rate of displacement of all the piles showed a rapid decrease in the initial stages of cyclic loading from high initial values to lower values. The rate of decrease, however, decreased until a low value was reached. This observation can be explained from the shear test results of Youd and Craven (1975). The results showed that most of the horizontal stress increase occurred during the first few cycles of shearing and the rate of increase decreased with increasing cycle number until the amount of increase per cycle was small. The increase in the horizontal stress is associated with an increase in the skin friction (see also chapter 2) which in turn would cause a reduced rate of displacement.

The rate of displacement-number of load cycles behaviour of all the piles are plotted in Figure 8.2. Owing to the different orders of magnitude of the rates of displacement, the results have been presented in logarithmic scales. The lower amplitude (10kN) piles, at all tested MCLVs, showed no tendency for the rate of displacement to increase after 108 000 cycles whereas the rate of the larger amplitude (30kN) piles increased after a relatively short period of cyclic loading. The significant difference between the lower (10kN and 20kN) and the higher (30kN) amplitudes again suggests that a critical amplitude of loading exists. The increase in the rate of displacement after the stable linear stage (also observed by Hanna et al., 1978) is associated with a degradation in the skin friction along the shaft of the piles.

There is a peculiar observation which is not typical to the creep behaviour of soils (Mitchell et al, 1968) or ground anchors (Jelinek and Scheele, 1978). The rate of displacement for the high amplitude piles approaches a peak value after which the rates drop off again. This increase to a maximum rate followed by a decrease is, however, in agreement with the experimental observations of Chan and Hanna (1980) and Hanna et al. (1978). A possible reason for the subsequent decrease is the increased densification under the pile tip after a large total displacement.

For the 30kN amplitude piles it can be seen that if the amplitude and the MCLV are of the same magnitude the rate of pile movement increases in the fewest number of load cycles.

For the low 10kN amplitude piles an increase in the MCLV results in a larger rate of displacement at a specific number of load cycles. However, for the 30kN amplitude piles the increase in the MCLV has the opposite effect. The pile at a MCLV of 30kN achieves higher rates of displacement in fewer numbers of cycles than both the 60kN MCLV and 90kN MCLV piles which show similar curves. This suggests the existence of a critical MCLV.

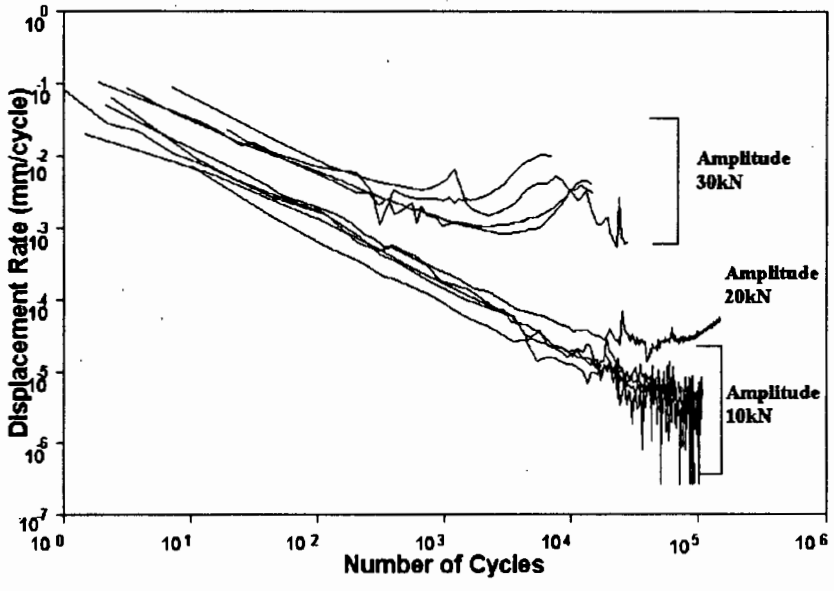

Figure 8.2 : Rate of displacement - number of cycles relationship of all test piles (logarithmic scale)

Cyclic Load-Displacement Response : The load-displacement response of the piles during one load cycle was presented in terms of the sand-pile stiffness modulus. At low amplitudes (10kN) the increase of the MCLV did not affect the rate of degradation of the stiffness modulus during cyclic loading, but only resulted in an increase in the magnitude of the average stiffness modulus. The modulus decreased only slightly as the number of cycles increased. An increase in the load amplitude, and hence strain amplitude, caused a decrease in the initial value of the stiffness modulus at the start of cyclic loading. The modulus then decreased with an increase in the number of load cycles, the rate of decrease being greater for higher amplitudes. This was particularly evident in the hysteretic response of the piles cyclically loaded at a MCLV of 60kN. This finding is supported by Kraft et al. (1981) and

Poulos (1981b) both of whom state that the cyclic stiffness decreases with increasing amplitude and number of cycles.

Ultimate Load Capacity after Cyclic Loading : Based on the results of these tests only a very general statement can be made regarding the ultimate load capacity of the piles after cyclic loading. The load amplitudes and MCLVs effect the ultimate loads of the piles after cyclic loading. Lower amplitudes result in higher final ultimate load capacities. An increase in the number of load cycles produces a decrease in the ultimate load of the piles. This is consistent with Poulos (1981b) who states that the ultimate load capacity decreases with increasing number of cycles and increasing amplitudes.

Skin Friction Distribution along Shaft : Examination of the piles with low amplitudes (10kN) revealed that the skin friction was mobilised at the pile base for high MCLVs, whereas at a lower MCLV the mobilisation occurred in the middle region of the shaft. Poulos (1981b) confirms this by stating that as the MCLV increases the soil stiffness degrades particularly near the top of the pile. Consequently more load is carried in the lower part of the pile. All the low amplitude test piles reached a certain skin friction distribution and maintained this 'equilibrium' throughout the test period.

Along the piles with high amplitudes (30kN) the peak of the skin friction distribution increased and moved progressively along the pile shaft towards the tip. Having reached the tip, the skin friction then degraded to reach an almost constant residual distribution. This stage of decreasing skin friction can be associated with a reduction in the normal stresses around the shaft. After the residual skin friction is attained any load must then be carried by the pile tip as the pile is sliding along its entire length and little or no increase in shearing resistance can be achieved (Appolonia and Romualdi, 1963). The point resistance then controls the piles behaviour from this stage of loading onwards.

The increase in the tip skin friction of pile 43 after 7080 cycles can be attributed to the high compression under the pile tip as the point resistance increases. The pressure causes arching of the sand around the tip which in turn results in an increase in the horizontal stresses along the lower sections of the pile shaft. The increase in horizontal stresses must

cause an increase in the side resistance near the tip which is shown at cycle 11 000. It should be noted that the displacements at this point are relatively large when compared to the pile diameter.

It was established that at a displacement of about 9.6% of the pile diameter the skin friction at the pile base began to decrease and the rate of displacement began to increase. This important observation supports the assumption of other writers that the pile has 'failed' at a displacement of about 10% of the pile diameter (Lee and Poulos, 1991; De Alba, 1983; Vesic, 1970). Thus, failure can be defined as the load or stage of loading at which a pile becomes unstable - ie. the skin friction starts to degrade and the rate of penetration increases.

Point Resistance of Pile : It was evident that the point resistance increased with increasing number of cycles. For the piles with 10kN amplitudes the point resistance rose to a certain maximum value and remained constant during subsequent cycles. On the other hand, piles with more destructive amplitudes (30kN) showed a continual increase in the point resistance due to the degradation of skin friction.

The magnitudes of the maximum point stresses at the end of cyclic loading were 2.86MPa for pile 53 and 8.4MPa for pile 52. These values are of the same order of magnitude as in the tests of De Alba (1983) where ultimate tip stresses of small model piles in sand were calculated to be 5.3MPa.

Analysis of hysteretic behaviour at pile tip : The analysis of the hysteretic behaviour at the pile tip was limited due to the availability of only four cyclically loaded instrumented piles. However, the trends established showed that the magnitudes of the elastic sand response below the pile tip during a cycle of loading were greater for the piles subjected to high amplitudes (30kN). The magnitudes also increased with an increase in the number of load cycles.

CHAPTER 9:
CONCLUSIONS

The experimental investigation presented in this report has concentrated on the behaviour of pressure-grouted piles subjected to cyclic loading in a moist sand medium. Owing to the large variety of variables involved here, an attempt was made to keep most of them constant and vary only two, namely the mean cyclic load level (MCLV) and the amplitude. The same soil conditions, pile installation methods and loading procedures were common to all the pile tests. The cyclic loading was stress-controlled and applied at a constant frequency and waveform (sinusoidal) in a one-way compressive mode.

In this way a highly controlled research procedure was developed which resulted in repeatable sand preparation, pile installation, load application and pile instrumentation techniques. The procedure produced consistent results which were analyzed in terms of the:

- static and cyclic load - displacement behaviour
- displacement - number of cycles relationship
- rate of displacement - number of cycles relationship
- sand-pile system stiffness modulus - number of cycles relationship
- load distribution and load transfer (skin friction) along the pile shaft during cyclic loading and the
- point resistance development during cyclic loading

The detailed results (presented in chapter 7) were summarised and discussed in chapter 8 and therefore it is not intended to repeat these observations in their entirety.

For each group of loading (MCLV and amplitude) compared, at least one instrumented pile was installed in order to obtain detailed information on the skin friction distributions. This

led to a good insight into the mechanisms of cyclic degradation which in turn provided explanations for the pile behavioural aspects investigated.

The low amplitudes (10kN or 5% of ultimate load) resulted in the skin friction along the pile shaft increasing to reach stable and constant distributions. Point resistance increased gradually to attain a constant value. Therefore, there was little penetration of the piles into the sand during large numbers of cycles. The rates of penetration decreased to reach almost constant and stable low values and the stiffness modulus displayed no significant degradation.

The higher amplitudes (30kN or 15% of ultimate load) caused the skin friction to reach peak values which progressively moved down the pile shafts during cyclic loading. When the peaks reached the pile base the skin friction along the entire shaft decreased to low residual values. The point resistance increased continuously. This degradation of the skin friction led to substantial increases in the displacement in a relatively few number of cycles. The rates of displacement were large and decreased to minimum values after which they rapidly increased to reach peak values. The stiffness moduli showed lower initial values than in the low amplitude cases and degraded rapidly with increasing numbers of cycles.

The point resistance increased with an increase in the number of cycles. More specifically, the magnitudes became larger when the skin friction reached low residual values. The pile behaviour was then controlled by the point resistance.

A significant observation was that at an overall pile head displacement of about 10% of the pile diameter the skin friction began to drop off and the rate of displacement increased. The ultimate loads after cyclic loading appeared to decrease with increasing amplitudes of loading and increasing numbers of cycles.

An increase in the MCLV produced slightly larger displacements in the low amplitude cases whereas for the high amplitudes an increase resulted in reduced displacements and rates of displacement at a specific number of cycles. The MCLV appeared to have little

effect on the degradation of the sand-pile system stiffness modulus although the average values increased with the MCLV. The skin friction was mobilised lower down the pile shaft for a larger MCLV.

Although the effects of the amplitude were seen to be more severe than that of the MCLV, it is essential to consider the combined effects of these two parameters. It is believed that either a critical MCLV or a critical amplitude exists in combination with the other cyclic variable (ie. amplitude or MCLV). With additional research, expanding on the different combinations of cyclic parameters, it is hoped that a full understanding of the combined effects of these parameters is achieved.

The findings of this research work compare favourably with those of many other authors of the respective research papers and the results contribute significantly to fill the gap in published literature on the behaviour of cyclically loaded pressure-grouted piles in sand. Comparisons of these results, possibly in non-dimensional form, with existing published experimental results may further enhance a greater understanding of the mechanisms of cyclic loading of piles in general. The wealth of experimental data that has been collected provides a basis for more detailed experimental and numerical analyses.

LIST OF REFERENCES

APPOLONIA, E.D. and ROMUALDI, J.P. 1963. Load Transfer in End-Bearing Steel Piles. ASCE, *Journal of Soil Mechanics and Foundations*, Vol. 89, No. SM2, pp. 1-25.

ASTM D698 - 78. 1987. *Annual book of ASTM Standards. Section 4 - Construction.* Vol 04.08, American Society for testing and materials, Philadelphia.

ASTM D4373 - 84. 1987. *Annual book of ASTM Standards. Section 4 - Construction.* Vol 04.08, American Society for testing and materials, Philadelphia.

BEA, R. 1992. Pile Capacity for Axial Cyclic Loading. ASCE, *Journal of Geotechnical Engineering*, Vol. 118, No. 1, pp. 34-50.

BORLAND. 1992. *Quattro Pro computer package*, Version 4.00, Borland International, Inc., California.

BRADLEY, J.M. 1988. Finite Element Analysis of Tests on Piles. BSc Thesis, University of Cape Town.

BS1377 - Part 2. 1990. *British Standard Methods of testing for Soils for Civil Engineering Purposes - Classification Tests.* British Standards Institution, London.

BS1881 - Part 116. 1983. *British Standard for Testing Concrete - Method for determination of the compressive strength of concrete cubes.* British Standards Institution, London.

BS1881 - Part 121. 1983. *British Standard for Testing Concrete - Method for determination of static modulus of elasticity in compression.* British Standards Institution, London.

CHAN, S. and HANNA, T.H. 1980. Repeated Loading on Single Piles in Sand. ASCE, *Journal of Geotechnical Engineering*, Vol. 106, No. GT2, pp. 171-187.

CODE OF PRACTICE, 1989. *Lateral Support in Surface Excavations.* The South African Institution of Civil Engineers, Geotechnical Division, Yeoville.

COOKE, R.W., PRICE, G. and TARR, K. 1979. Jacked piles in London Clay: a study of load transfer and settlement under working conditions. *Geotechnique*, Vol. 29, No. 2, pp. 113-147.

CORNELIUS, V. and MEHLHORN, G. 1982. Tragfähigkeitsuntersuchungen im Verankerungsbereich von Verpreβankern und Pfählen mit keinem Durchmesser für den Anwendungsbereich Lockergestein. *Research report No. 46*, Technischen Hochschule Darmstadt.

COWBURN, S.J. 1990. Full Scale Pile Tests using an Electronically Controlled Load Actuator. BSc Thesis, University of Cape Town.

COWBURN, S.J. and SCHEELE, F.S. 1993. Behaviour of Cyclically Loaded Instrumented Piles. *Proc. 2nd Southern African Young Geotechnical Engineers Conference*, Cape Town.

CUELLAR, V., BAZANT, Z.P., KRIZEK, R.J. and SILVER, M.L. 1977. Densification and Hysteresis of Sand under Cyclic Shear. ASCE, *Journal of Geotechnical Engineering*, Vol. 103, No. GT5, pp. 399-416.

DESAI, C.S., DRUMM, E.C. and ZAMAN, M.M. 1985. Cyclic Testing and modelling of Interfaces. ASCE, *Journal of Geotechnical Engineering*, Vol. 111, No. 6, pp. 793-815

DE ALBA, P.A. 1983. Pile Settlement in Liquefying Sand Deposit. ASCE, *Journal of Geotechnical Engineering*, Vol. 109, No. 9, pp. 1165-1179.

HANNA, T.H., SIVAPALAN, E. and SENTURK, A. 1978. The Behaviour of Dead Anchors Subjected to Repeated and Alternating Loads. *Ground Engineering*, Vol. 2, No. 3, pp. 28-40.

HARDIN, B. and DRNEVICH, V.P. 1972. Shear Modulus and Damping in Soils:Design equations and curves. ASCE, *Journal of Soil Mechanics and Foundations Division*, Vol. 98, No. SM7, pp. 667-691.

HEAD, K.H. 1982. *Manual of Soil Laboratory Testing*. Vol. 2, Halsted Press, New York.

HEAD, K.H. 1986. *Manual of Soil Laboratory Testing*. Vol. 3, Pentech Press Limited, Devon.

HEWLETT PACKARD. 1981. Practical Strain Gage Measurements. *Application note 290-1*, Colorado, U.S.A.

HEWLETT PACKARD. 1982. *Model 3497A Data Acquisition/Control Unit - operating, programming and configuration manual.* Hewlett Packard, Colorado, U.S.A.

JELINEK, R. and SCHEELE, F. 1978. Das Kriechverhalten von Verpressankern. *Eigenverlag Bundesministerium für Verkehr*, Bonn, West Germany.

KORECK, H.W. and SCHWARZ, P. 1988. Axial cyclic loaded piles. *Proc. 1st IGSDF*, Balkema, Rotterdam, pp. 395-399.

KRAFT, L.M., COX, W.R. and VERNER, E.A. 1981. Pile Load Tests: Cyclic Loads and Varying Load Rates. ASCE, *Journal of Geotechnical Engineering*, Vol. 107, No. GT1, pp. 1-19.

KYOWA. 1985. *Strain Gauge Instruction Manual*, Kyowa Limited, Japan.

LEE, C. Y. and POULOS, H.G. 1991. Test on Model Instrumented Grouted Piles in Offshore Calcareous Soil. ASCE, *Journal of Geotechnical Engineering*, Vol. 117, No. 11, pp. 1738-1753.

LEHANE, B.M., JARDINE,R.J., BOND,A.J. and FRANK, R. 1993. Mechanisms of Shaft Friction in Sand from Instrumented Pile Tests. ASCE, *Journal of Geotechnical Engineering*, Vol. 119, No. 1, pp. 19-35.

MITCHELL, J.K, CAMPANELLA, R.G. and SINGH, A. 1968. Soil Creep as a Rate Process. ASCE, *Journal of Soil Mechanics and Foundations*, Vol. 94, No. SM1, pp. 231-253.

POTYONDY, J.G. 1961. Skin Friction between Various Soils and Construction Materials. *Geotechnique*, Vol. XI, pp. 339-353.

POULOS, H.G. 1981a. Some Aspects of Skin Friction of Piles in Clay under Cyclic Loading. SEASSE, *Geotechnical Engineering*, Vol. 12, No. 1, pp. 1-17.

POULOS, H.G. 1981b. Cyclic Axial Response of Single Pile. ASCE, *Journal of Geotechnical Engineering*, Vol. 107, No. GT1, pp. 41-58.

POULOS, H.G. 1987. Analysis of Residual Stress Effects in Piles. ASCE, *Journal of Geotechnical Engineering*, Vol. 113, No. 3, pp. 216-229.

POULOS, H.G. 1988. Cyclic Stability Diagram for Axially Loaded Piles. ASCE, *Journal of Geotechnical Engineering*, Vol. 114, No. 8, pp. 877-895.

POULOS, H.G. 1989. Cyclic Axial Loading Analysis of Piles in Sand. ASCE, *Journal of Geotechnical Engineering*, Vol. 115, No. 6, pp. 836-852.

PRAKASH, S. 1981. *Soil Dynamics*. McGraw-Hill, Inc., USA.

REESE, L.C., HUDSON, W.R. and VIJAYVERGIYA, V.N. 1969. An Investigation of the Interaction between Bored Piles and Soil. *Proc. 7th ICSMFE*, Mexico, Vol. 2, pp. 211-215.

RODIO, 1989. Documentation on Compaction Grouting, *Internal Report*, Rodio (Cape).

ROSMANITH, H.P. 1993, Personal communication.

SABS 0100:1. 1992. *South African Standards - Code of Practice - The structural use of concrete. Part 1 : Design.* The council of the South African Bureau of Standards.

SCHEELE, F., SELLERS, E.J. and COWBURN, S.J. 1991. Full Scale Pile Testing under Controlled Conditions. *Proc. 10th Regional Conf. for Africa on SMFE*, Maseru, Vol. 1, pp 223-227, Balkema, Rotterdam.

SCHWAEBLE, R. 1991. Determination of Ultimate Bearing Capacity Beneath Various Foundation Specimens. BSc Thesis, University of Cape Town.

SILVER, M.L. and SEED, H.B. 1971a. Deformation Characteristics of Sands under Cyclic Loading. ASCE, *Journal of Soil Mechanics and Foundations*, Vol. 97, No. SM8, pp. 1081-1098.

SILVER, M.L. and SEED, H.B. 1971b. Volume changes in sands during cyclic loading. ASCE, *Journal of Soil Mechanics and Foundations*, Vol. 97, No. SM9, pp. 1171-1182.

TERZAGHI, K. and PECK, R. 1948. *Soil Mechanics in Engineering Practice.* John Wiley and Sons, Inc., New York.

TOUMA, F.T. and REESE, L.C. 1974. Behaviour of Bored Piles in Sand. ASCE, *Journal of Geotechnical Engineering*, Vol. 100, No. GT7, pp. 749-761.

TROCHANIS, A.M., BIELAK, J. and CHRISTIANO, P.P. 1987. Hysteretic Dissipation of Piles under Cyclic Axial Load. ASCE, *Journal of Geotechnical Engineering*, Vol. 113, No. 4, pp. 335-350.

VESIC, A.S. 1970. Tests on Instrumented Piles, Ogeechee River Site. ASCE, *Journal of Soil Mechanics and Foundations*, Vol. 96, No. SM2, pp. 561-584.

VAN DER VEEN. 1953. Bearing Capacity of Piles. *Proceedings of the 3rd ICSMFE*, Vol. 2, pp. 84-90.

WARNER, J. 1978. Compaction Grouting - A Significant Case History, ASCE, *Journal of Geotechnical Engineering*, Vol. 104, No. GT7, pp. 837-847.

YOUD, T.L. 1972. Compaction of Sands by Repeated Shear Straining. ASCE, *Journal of Geotechnical Engineering*, Vol. 98, No. SM7, pp. 709-725.

YOUD, T.L. and CRAVEN, T.N. 1975. Lateral Stress in Sands during Cyclic Loading. ASCE, *Journal of Geotechnical Engineering*, Vol. 101, No. GT2, pp. 217-221.

APPENDIX A

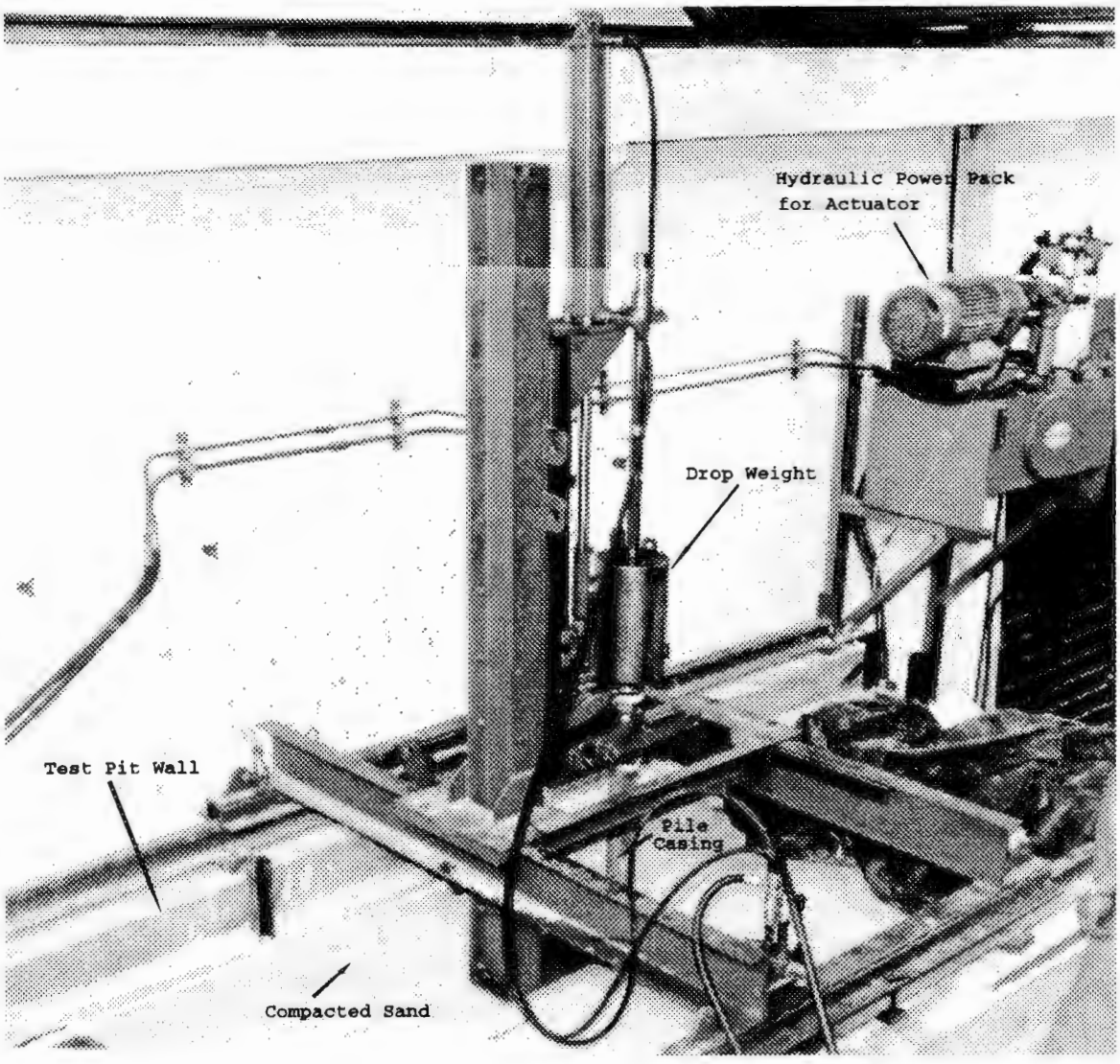

Figure A1 : Scanned image of photograph of drop-weight pile driver

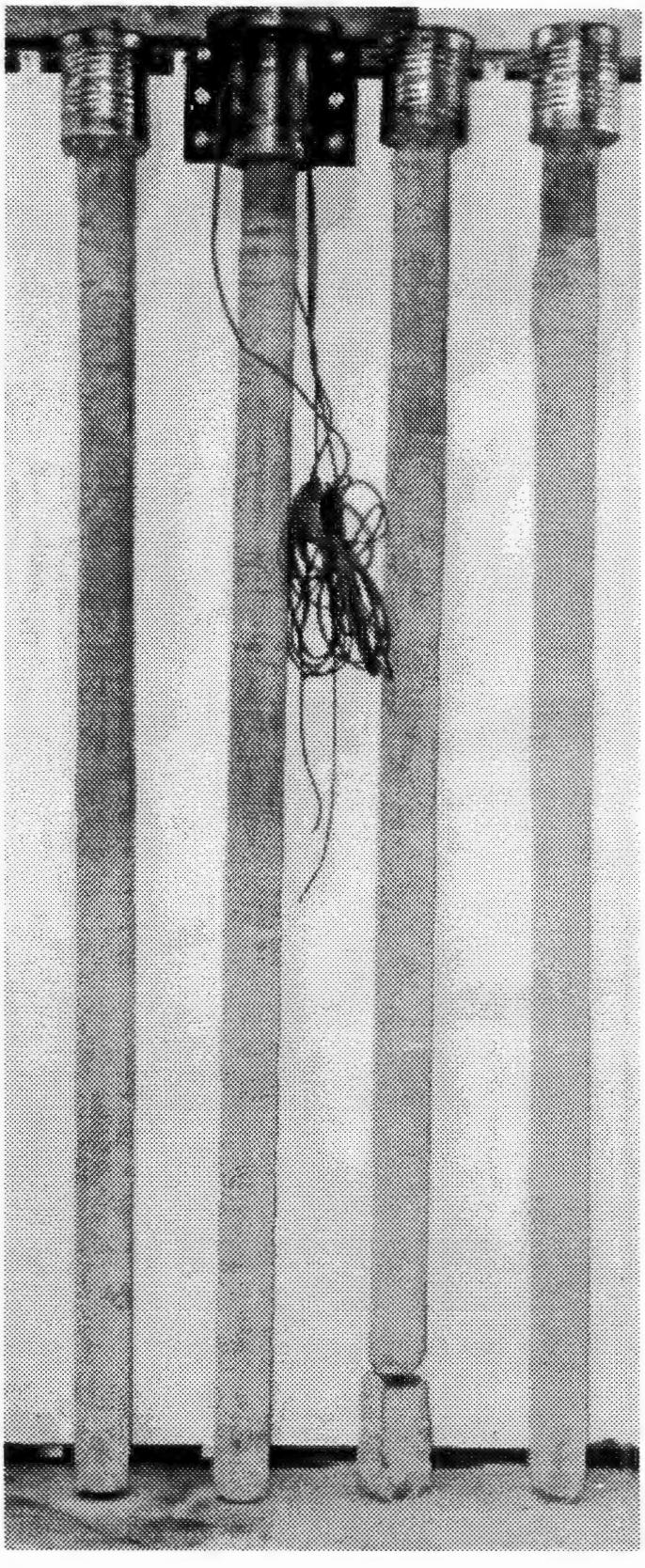

Figure A2 : Scanned image of photograph of piles in Series 3 (from right to left are piles 31 to 34)

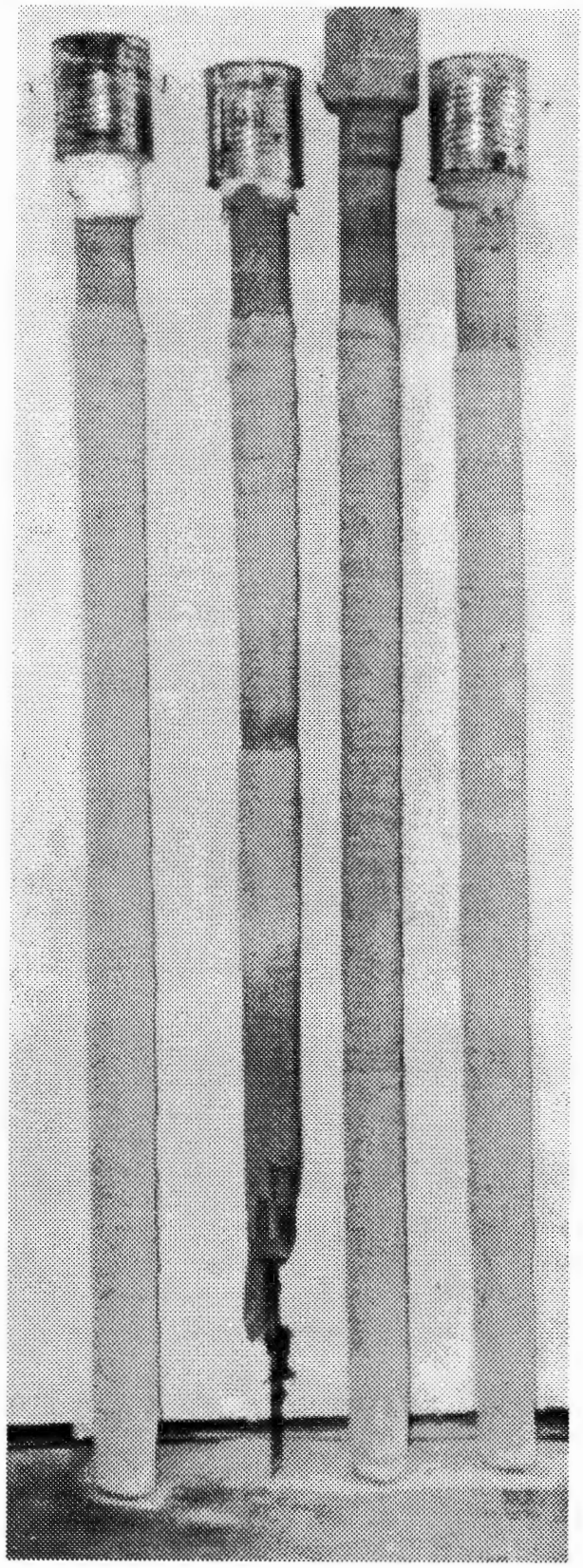

Figure A3 : Scanned image of photograph of piles in Series 4 (from left to right are piles 41 to 44)

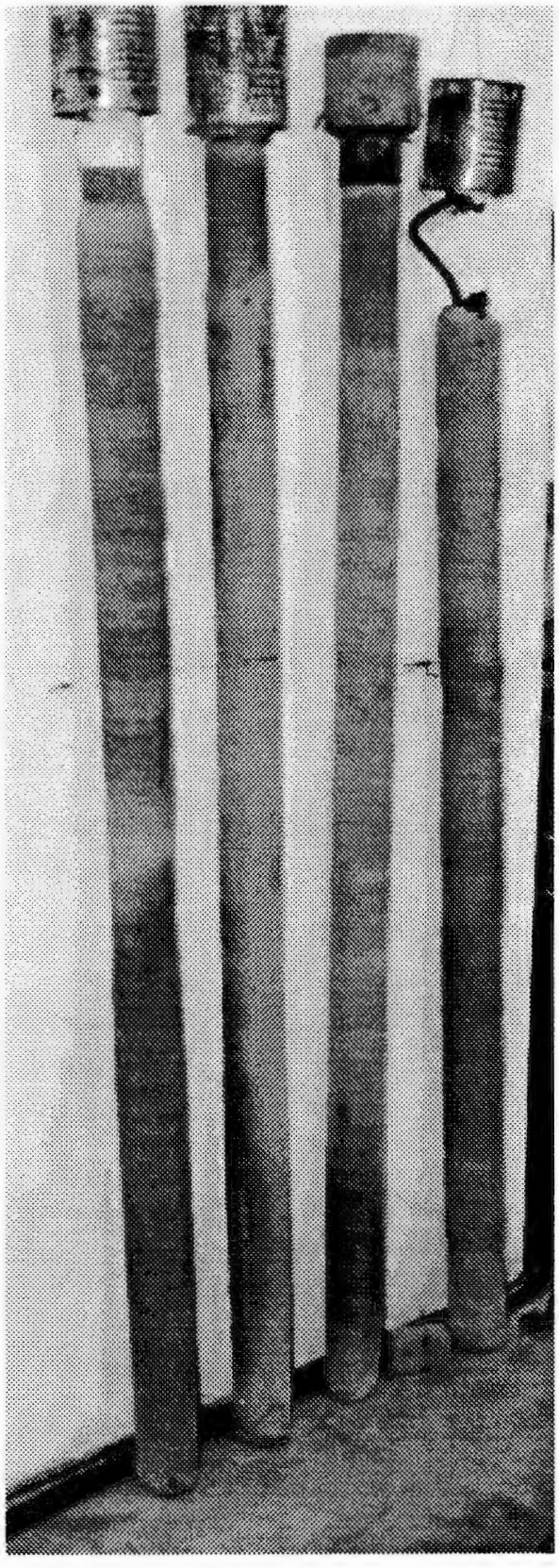

Figure A4 : Scanned image of photograph of piles in Series 5 (from right to left are piles 51 to 54)